INTERNATIONAL ATOMIC ENERGY AGENCY
UNITED NATIONS EDUCATIONAL, SCIENTIFIC AND CULTURAL ORGANIZATION

INTERNATIONAL CENTRE FOR THEORETICAL PHYSICS
34100 TRIESTE (ITALY) - P.O.B. 586 - MIRAMARE - STRADA COSTIERA 11 - TELEPHONES: 224281/2/3/4/5/6
CABLE: CENTRATOM - TELEX 460392-1

SMR/111 - 5

SECOND SUMMER COLLEGE IN BIOPHYSICS

30 July - 7 September 1984

1. Principles of Magnetic Resonance
2. The Overhauser Effect
3. The Two Dimensional Overhauser Effect
4. Iminoproton Exchange and the Stability and Dynamics of Double Helices

C.W. HILBERS
Faculteit der Wiskunde en Natuurwetenschappen
Katholieke Universiteit
Toernooiveld
6525 ED Nijmegen
The Netherlands

I PRINCIPLES OF MAGNETIC RESONANCE

A. QUANTUM MECHANICAL DESCRIPTION

The atomic nuclei possess angular momentum or spin. In addition, atomic nuclei bear charge and their spinning produces a magnetic moment (microscopic bar magnet).

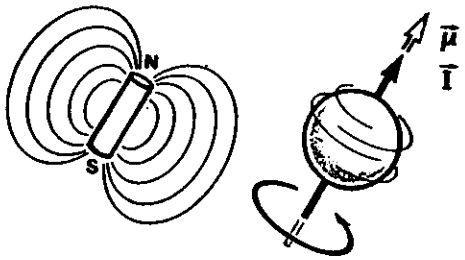

Figure 1

The magnetic moment, $\vec{\mu}$, is proportional to the spin angular momentum, $\vec{I}$:

$$\vec{\mu} = \gamma \hbar \vec{I} \qquad (1)$$

γ = gyromagnetic ratio

$\hbar = h/2\pi$; h = Planck's constant

In absence of a magnetic field spins are randomly oriented.

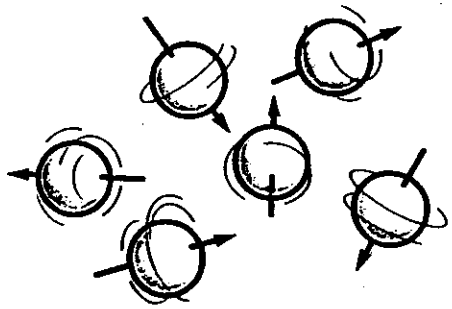

Figure 2

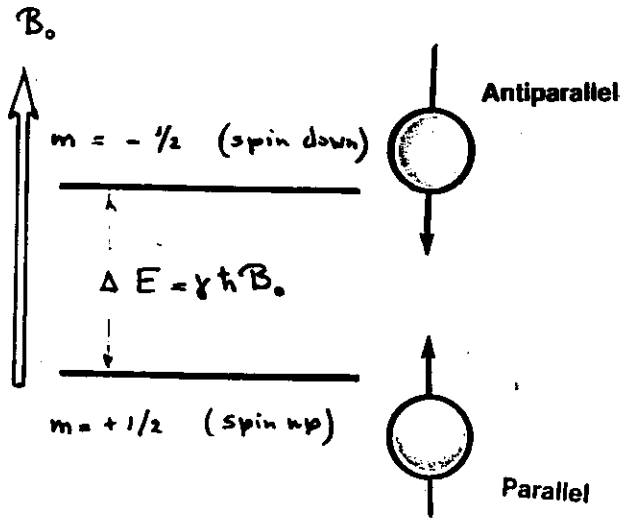

Figure 3

Exposed to a magnetic field the spins are oriented. (example for spin-½ system)

According to quantum mechanics the energy corresponding to different orientations is discrete:

$$E = -\gamma \hbar B_0 m \qquad (2)$$

m is the projection of on the z-axis (the direction of the magnetic field B_0)

m can have the following values:

$$m = I, I-1, \ldots\ldots\ldots, -I. \qquad (3)$$

Atomic nuclei with $I = \frac{1}{2}$ (spin $\frac{1}{2}$) such as ^1H, ^{13}C, ^{19}F and ^{31}P have only two energy states ($m = \pm \frac{1}{2}$). These spins are oriented parallel (spin up) and antiparallel (spin down) to the magnetic field. (see Fig 3).

The energy separation between the two states is:

$$\Delta E = \gamma \hbar B_0 \qquad (4)$$

Transitions between the two states can be induced by electromagnetic radiation with a frequency, ν_0, related to the energy separation by:

$$\Delta E = h\nu_0 = \hbar\omega_0 \qquad (5)$$

Equations (4) and (5) yield:

$$\boxed{\omega_0 = \gamma B_0} \qquad (6)$$

This is the <u>Larmor relationship</u>

ω_0 is the <u>resonance frequency</u>

The combination of frequency and magnetic field strength fullfilling equations (6) gives rise to a resonance signal.

Figure 4

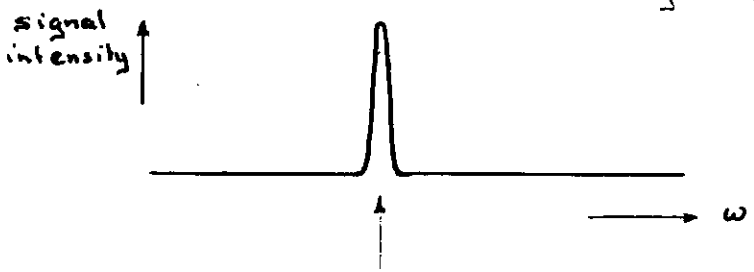

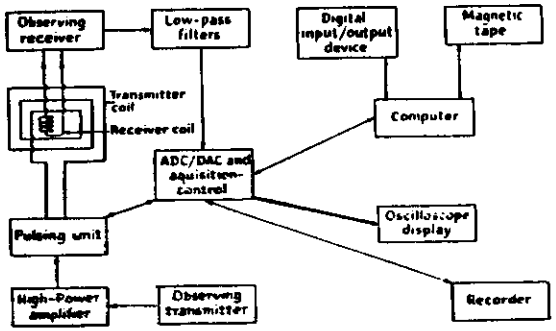

Figure 5. Schematic diagram of a typical NMR pulse spectrometer

B. ENERGY ABSORPTION, T_1-RELAXATION, SATURATION

Consider a spin-$\frac{1}{2}$ system (protons). Number of protons with spin up is N_+, number of protons with spin down is N_-. At equilibrium the relative population of the energy levels is according to Boltzmann's law

$$\frac{N_-}{N_+} = e^{-\Delta E/kT} \qquad (7)$$

Changes in the populations of the energy levels

Fig. 6

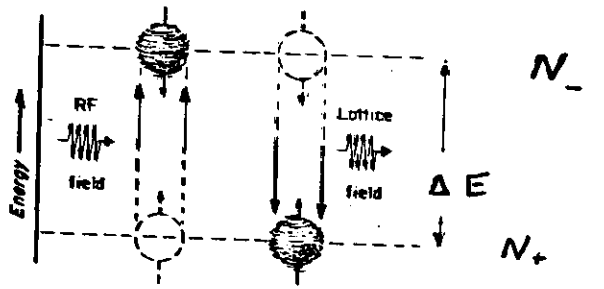

may be induced when the spin system is irradiated (radiation with the proper frequency) and energy is absorbed from the radiation field (the radio frequency (rf) field). In this way spins may be promoted from the ground state to the excited state. Spin lattice relaxation (i.e. T_1 - relaxation) may re-establish the equilibrium situation (Fig 6).

Changes in the populations under the influence of the rf. field can be described by the rate equations:

$$\frac{dN_+}{dt} = -W(N_+ - N_-) \qquad (8a)$$

$$\frac{dN_-}{dt} = W(N_+ - N_-) \qquad (8b)$$

Using the linear combination of eqns. (8)

$$\frac{d(N_+ - N_-)}{dt} = -2W(N_+ - N_-) \qquad (9)$$

yields an expression for the time dependence of the magnetization (along the applied magnetic field)

$$\frac{dM_z}{dt} = -2WM_z \qquad (10)$$

where use has been made of

$$\mu_z = \tfrac{1}{2}\gamma\hbar \qquad (11)$$

$$M_z = \sum_i \mu_{zi} = \tfrac{1}{2}\gamma\hbar(N_+ - N_-) \qquad (12)$$

W is the induced transition probability. Integration of eq (10) yields

$$M_z = M_z(0)\, e^{-2Wt} \qquad (13)$$

9

Note that for long times (t) M_z becomes zero, i.e. $N_+ - N_-$ becomes zero. This is called saturation.

T_1 - relaxation processes may drive the spin system back to equilibrium. This process is described by the following rate equations

$$\frac{dN_+}{dt} = -W_r(N_+ - N_+^\circ) + W_r(N_- - N_-^\circ) \quad (14$$

$$\frac{dN_-}{dt} = W_r(N_+ - N_+^\circ) - W_r(N_- - N_-^\circ) \quad (14$$

W_r is the transition probability arising from the relaxation process; N_+° and N_-° are the equilibrium populations of the ground state and excited state respectively

10

Eqns (14a) and (14b) can be combined to:

$$\frac{d(N_+ - N_-)}{dt} = -2W_r\{(N_+ - N_-) - (N_+^\circ - N_-^\circ)\} \quad (15)$$

which yields the time dependence of the magnetization:

$$\frac{dM_z}{dt} = -2W_r(M_z - M_z^\circ) \quad (16)$$

where M_z° is the equilibrium magnetization. $2W_r \equiv T_1^{-1}$

T_1 is the spin lattice relaxation time. Integration of Eq. (16) yields:

$$M_z = M_z^\circ + A e^{-t/T_1} \quad (17)$$

A is an integration constant depending on the initial conditions of the experiment. If at $t=0$ the spin system was saturated

$$M_z = M_z^\circ(1 - e^{-t/T_1}) \quad (18)$$

This time dependence is shown in Figure 7

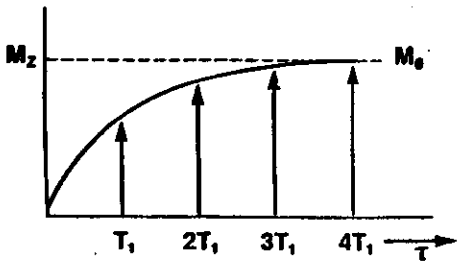

In the presence of a constant rf field and spin lattice relaxation the time dependence of the magnetization is :

$$\frac{dM_z}{dt} = -2W M_z - \frac{M_z - M_z^\circ}{T_1} \qquad (19)$$

If the rf field is present sufficiently long a steady state is reached so that $dM_z/dt = 0$. Hence

$$M_z = \frac{M_z^\circ}{1 + 2WT_1} \qquad (20)$$

Only for $2WT \ll 1$ $M_z = M_z^\circ$.

For $2WT_1 \gg 1$, i.e. $2W \gg T_1^{-1}$ M_z approaches zero. Hence when the relaxation processes cannot compete with the induced transition probabilities saturation sets in.

C. CLASSICAL DESCRIPTION, PULSE NMR, T_2, RELAXATION

The magnetic field, $\vec{B}$, produces a torque, $\vec{L}$, on the nuclear magnetic moment $\vec{\mu}$:

$$\vec{L} = \vec{\mu} \times \vec{B} \tag{21}$$

The magnetic moment arises from the spin angular momentum, $\vec{J} = \hbar \vec{I}$, and the nuclear charge. The rate of change of the angular momentum is:

$$\frac{d\vec{J}}{dt} = \vec{L} \tag{22}$$

so that

$$\frac{d\vec{\mu}}{dt} = \vec{\mu} \times \gamma \vec{B} \tag{23}$$

where use has been made of

$$\vec{\mu} = \gamma \vec{J} \tag{24}$$

Equation (23) holds regardless whether or not $\vec{B}$ is time dependent. When $\vec{B}$ is time independent analysis of eq. (13) shows that the magnetic moment precesses around the magnetic field with the Larmor frequency (Fig 8 a vide infra)

The sum

$$\sum_i \mu_{zi} = M_z \tag{25}$$

(z-axis is along the applied magnetic field)

All nuclear magnetic moments are out of phase so that there is no magnetization in the x y plane. In practice the equation of motion of the nuclear spins is defined in a frame rotating

around the static field $\vec{B}_0$ with an angular velocity

$$\vec{\Omega} = -\omega \vec{k} \qquad (26)$$

where $\vec{k}$ is the unit vector along the direction of $\vec{B}_0$. The time derivative of the magnetic moment in the laboratory frame is related to that in the rotating frame by

$$\frac{d\vec{\mu}}{dt} = \frac{\delta \vec{\mu}}{\delta t} + \vec{\Omega} \times \vec{\mu} = \vec{\mu} \times \gamma \vec{B} \qquad (27)$$

where $\delta\vec{\mu}/\delta t$ is the derivative in the rotating frame.

From this result it follows that

$$\frac{\delta \vec{\mu}}{\delta t} = \vec{\mu} \times (\gamma \vec{B} + \vec{\Omega}) \qquad (28)$$

Define an effective field $\vec{B}_{eff}$:

$$\vec{B}_{eff} = \vec{B} + \frac{\vec{\Omega}}{\gamma} \qquad (29)$$

Then

$$\frac{\delta \vec{\mu}}{\delta t} = \vec{\mu} \times \gamma \vec{B}_{eff} \qquad (30)$$

Thus $\vec{\mu}$ precesses around the effective magnetic field. When

$$\vec{B} = B_0 \vec{k} \qquad (31)$$

the static magnetic field and

$$\vec{\Omega} = -\gamma B_0 \vec{k} \qquad (32)$$

then

$$\frac{\delta \vec{\mu}}{\delta t} = 0 \qquad (33)$$

which means that $\vec{\mu}$ remains fixed with respect to the rotating field; in other words (combining Eq. 26 and 32) $\vec{\mu}$ is rotating around $\vec{B}_0$ with the Larmor frequency.

17

We proceed by adding to the static field an alternating field which rotates around the z-axis with a frequency equal to that of the rotating frame (see Fig 9a):

$$\vec{B}_1 = B_1 (\vec{i}\cos\Omega t + \vec{j}\sin\Omega t) \qquad (34)$$

If in the rotating frame $\vec{B}_1$ is directed along the x-axis one finds

$$\frac{\delta \vec{\mu}}{\delta t} = \vec{\mu} \times \gamma \left\{ \vec{k} B_0 + \vec{i} B_1 + \frac{\Omega \vec{k}}{\gamma} \right\} \qquad (35)$$

In this case

$$\vec{B}_{eff} = \vec{k} B_0 + \frac{\Omega \vec{k}}{\gamma} + \vec{i} B_1 \qquad (36)$$

Summing over all nuclear moments in the sample yields:

$$\frac{\delta \vec{M}}{\delta t} = \vec{M} \times \gamma \vec{B}_{eff} \qquad (37)$$

18

When

$$\vec{\Omega} = -\omega \vec{k} \qquad (\omega = \text{Larmor frequency}) \qquad (38)$$

$$\vec{B}_{eff} = \vec{i} B_1 \qquad (39)$$

Thus in the rotating frame the magnetization will turn about $\vec{B}_1$. Assume that at $t=0$ the magnetization is along the z-axis then $\vec{M}$ will rotate in the yz plane. The rotation frequency is

$$\omega_r = \gamma B_1 \qquad (40)$$

Since

$$\omega_r = d\theta / dt \qquad (41)$$

(θ is angle between $\vec{M}$ and z-axis) it follows that

$$\theta = \gamma B_1 t \qquad (42)$$

Hence by employing an alternating field B_1 for a certain time the magnetization, directed initially along the z-axis, can be rotated parallel to the y-axis (in the rotating frame). In other words a 90° pulse is applied (see Fig. 8b)
After this pulse, with only the static field present, the magnetization in the xy plane precesses about the z-axis (static field) (see Fig. 8c)

Figure 8

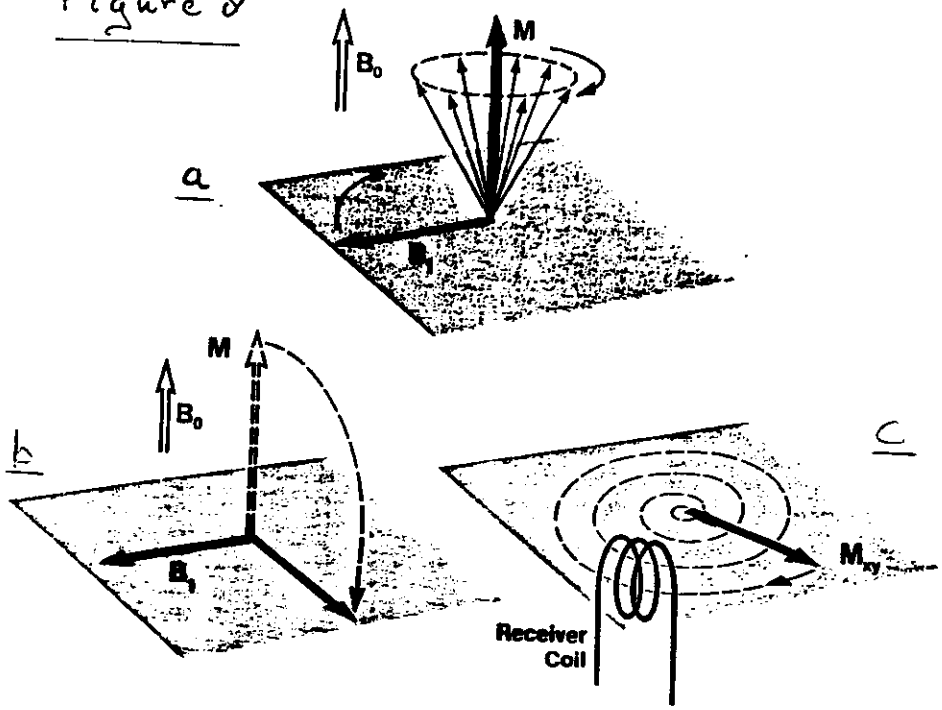

This gives rise a signal, picked up by the receiver coil, the so called free induction decay (see Fig.)

Figure 9 Free induction decay

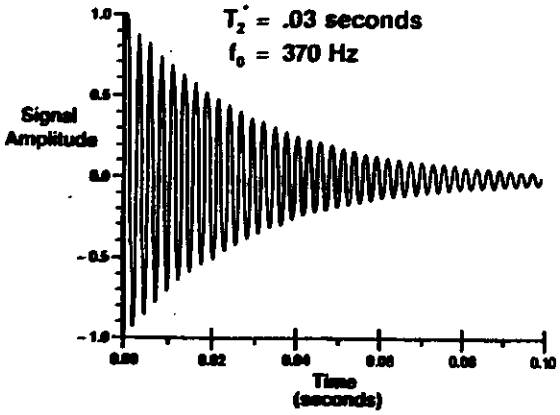

Fourier transformation of the free induction decay (FID) gives rise to the absorption (NMR) spectrum, see below

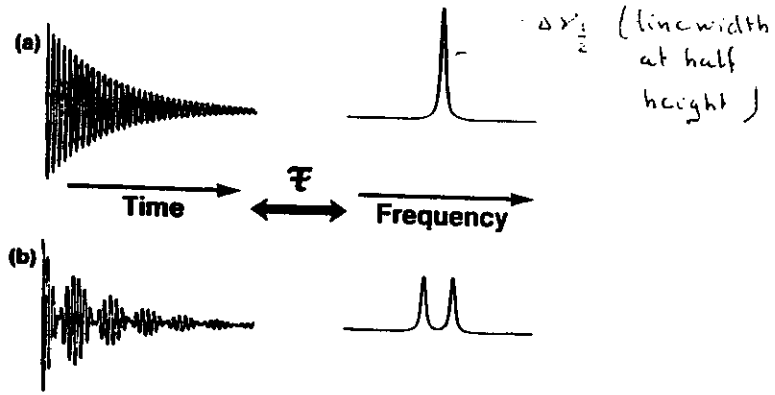

Figure 10 Fourier transformation of FID.

It is seen that the magnetization in the x y plane (Fig 9c) and therefore the free induction decay (Fig. 9 and 10) is damped.

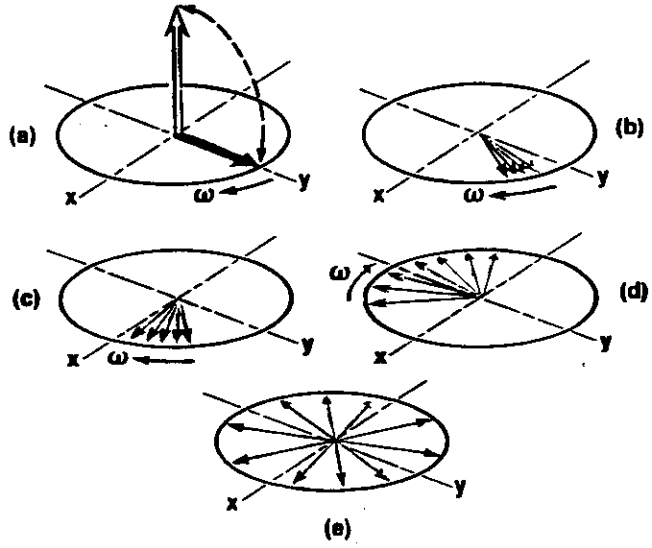

Figure 11: Dephasing of spins after a 90° pulse.

The time characteristic for the damping is T_2. It characterizes the so called spin-spin relaxation which causes a dephasing of the spins in the x-y plane (Fig 11).

T_2 characterizes the linewidth of the resonance:

$$\pi \Delta\nu_{\frac{1}{2}} = T_2^{-1} \qquad (43)$$

where $\Delta\nu_{\frac{1}{2}}$ is the linewidth at half height (Fig in).

Introduction of the spin-lattice (T_1) and spin-spin relaxation (T_2) in the equation of motion of the magnetization (Eq 37) yields for the component along the axes in the rotating frame

$$\frac{\delta M_x}{\delta t} = (\omega_0 - \omega) M_y - \frac{M_x}{T_2} \qquad (44a)$$

$$\frac{\delta M_y}{\delta t} = -(\omega_0 - \omega) M_x + \gamma M_z B_1 - \frac{M_y}{T_2} \qquad (44b)$$

$$\frac{\delta M_z}{\delta t} = -\gamma M_y B_1 - \frac{M_z - M_z^\circ}{T_1} \qquad (44c)$$

These are the famous Bloch equations

D. CHEMICAL SHIFTS

At the site of the nucleus the magnetic field will not be equal to B_0; the latter is screened somewhat by electrons surrounding the nucleus. As a result the resonance frequency of this nucleus is

$$\omega = \gamma (1 - \sigma) B_0 \qquad (45)$$

where σ is a shielding factor (the chemical shift) which is characteristic for the chemical group of which the considered proton (nucleus) is part. Proton chemical shifts of different groups are summarized in the Table 1 (groups of nucleic acids were taken as examples)

Table 1

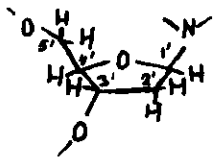

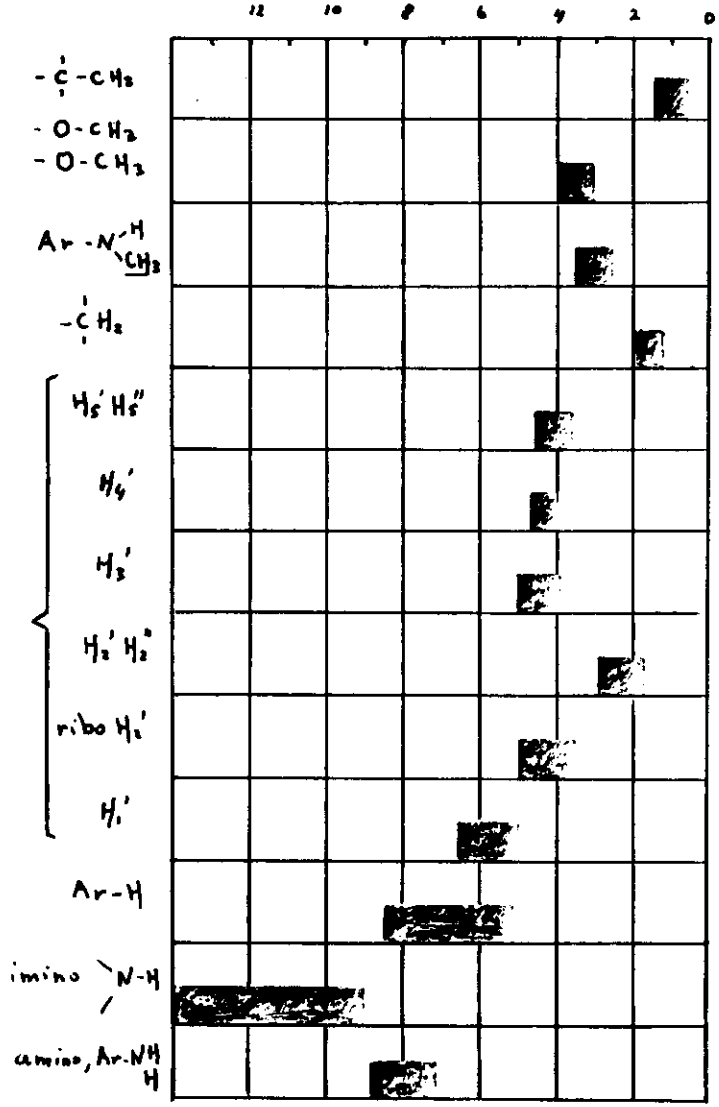

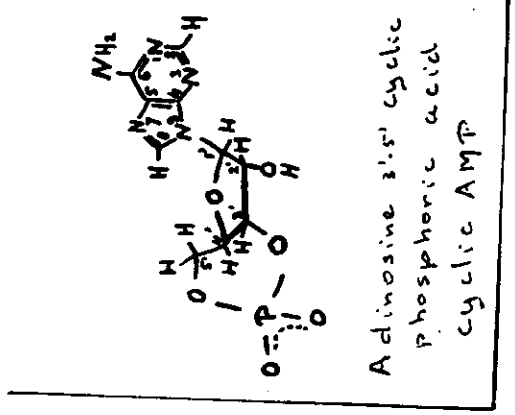

Adenosine 3',5' cyclic phosphoric acid
cyclic AMP

Fig 12.

Figure 12

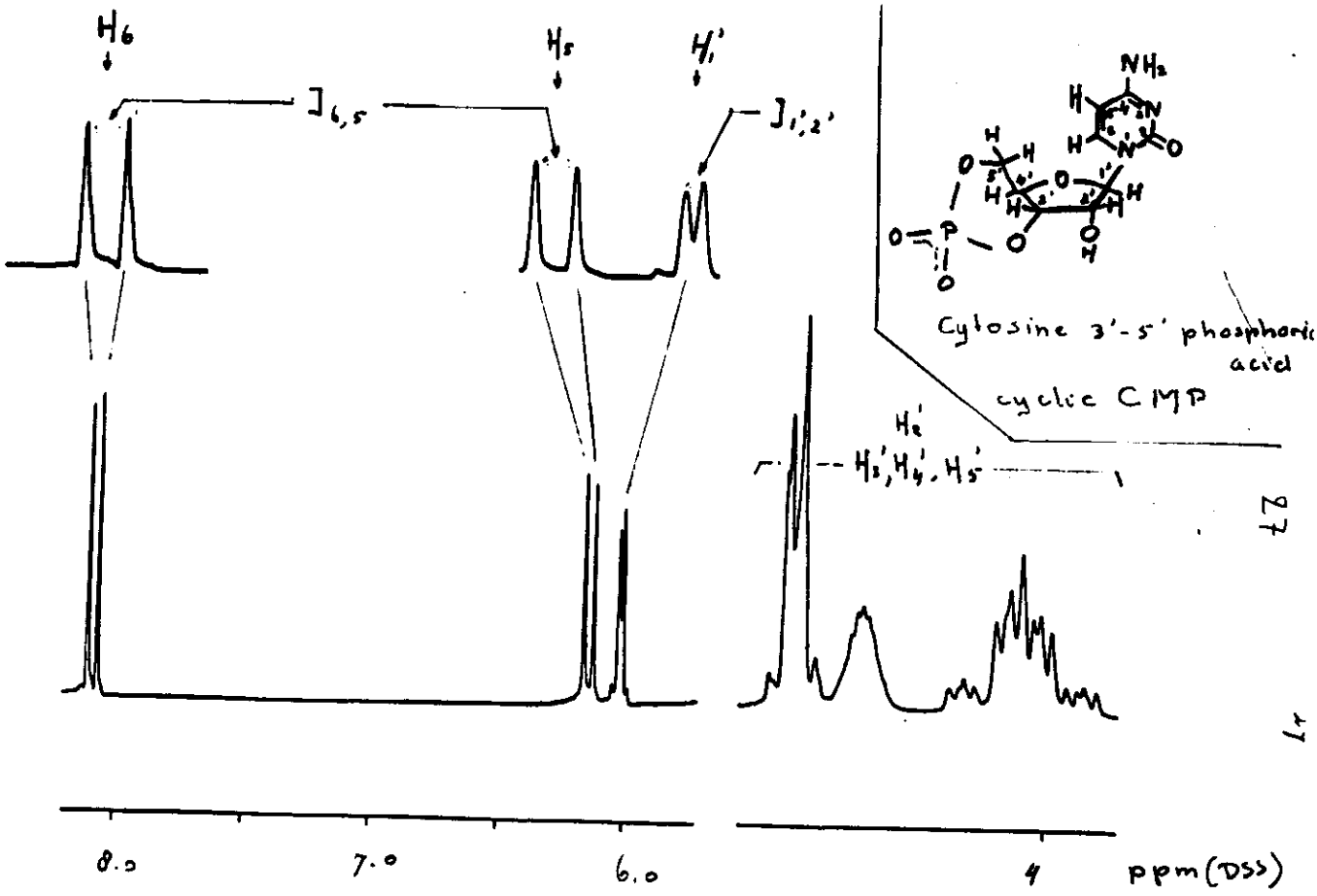

27

Figure 13

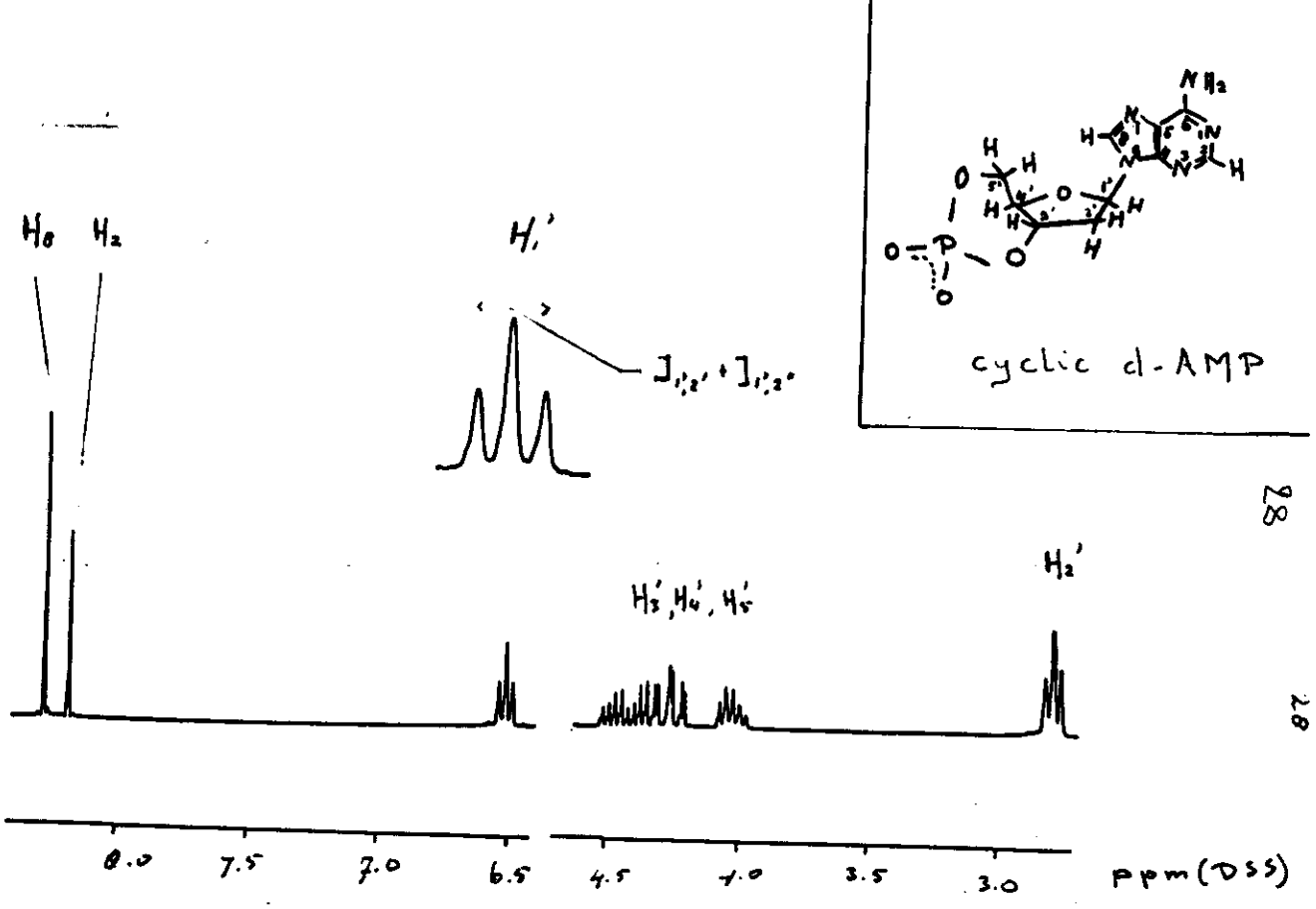

28

The chemical shift does not only depend on the chemical characteristics of a particular group, but also on the character of surrounding groups and therefore on the structure of the molecule. An example is given in Fig 15. Also the temperature and concentration may influence the resonance position. An example is given in Fig. 16 were the temperature and concentration is given of the H_1' and H_8 chemical shifts of the adenine moiety in m_2^6 A-U molecule (Hartel et. al. Eur. J. Biochem. 129, 343 (1982))

Another example are the changes in resonance positions presented

Figure 15. Part of the 500 MHz spectrum of m_2^6 Ap U p m_2^6 Ap U which clearly shows different positions for similar protons in different subunits (Hartel et al. (1981) Nucleic Acids Research 9, 1405).

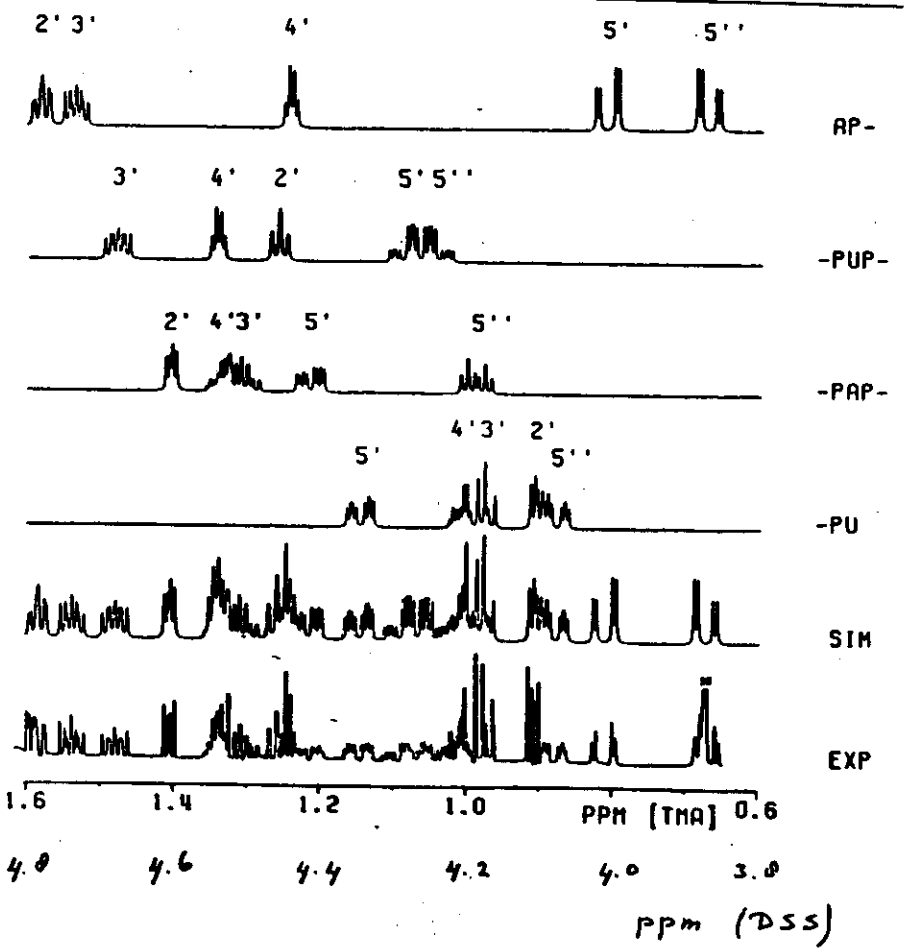

31

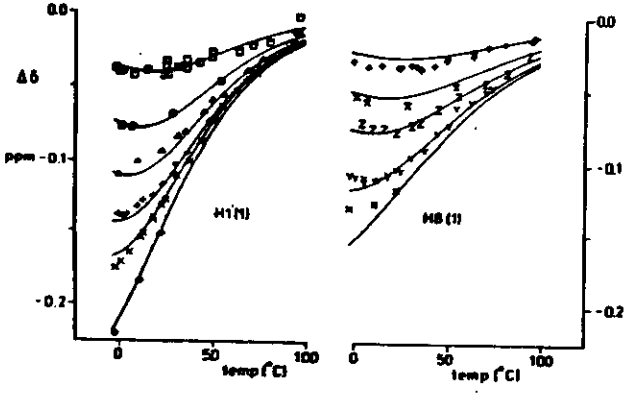

Figure 16

Influence of temperature and concentration on the chemical shift of the H_1' and $H8$ of m_2^6A-U

Figure 17 Influence of helix to coil transition on chemical shifts.

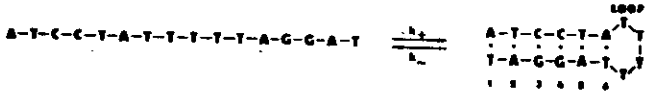

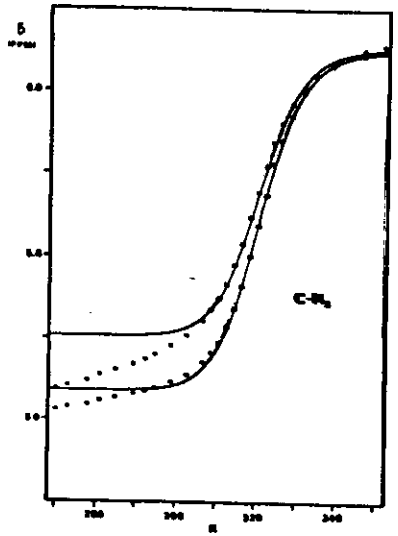

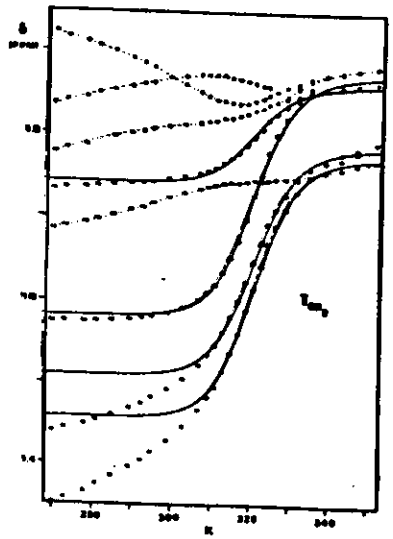

32

in Fig. 17 These shifts monitor the helix coil transition of the hexadecanucleotide

A T C C T A T T T T A G G A T

Of particular importance is the so called ringcurrent shift induced by the bases. The π-electrons of aromatic rings are not localized at particular carbon atoms but may so to speak move around the ring giving rise to ring current effects. Up and down the plane of the ring this results in a shielding effect (see Fig 18 g); in the plane there is a deshielding effect. The ring current (movement of the electrons) is induced by the applied magnetic field (see Fig 18)

33

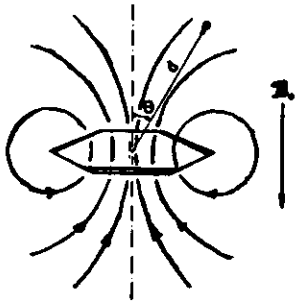

Figure 19 Magnetic ring current field giving rise to ring current shifts induced in aromatic rings by an external field B_o applied perpendicular to the ring

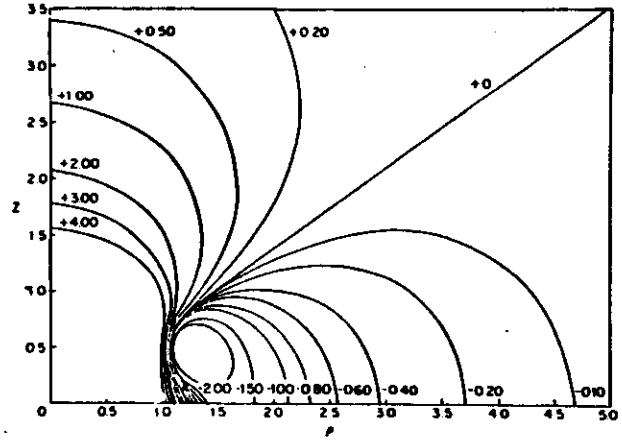

Figure 18 Shielding zone about a benzene ring. The plot represents one quadrant of a plane through the center of the ring normal to the ring plane. Origin of the plot is at the ring center; ρ axis is in the ring plane. ρ and z are in units of 1.39 Å.

Iso shielding lines are in ppm; positive numbers indicate shifts to higher fields

34

This is the main reason for the dispersion in resonance position of e.g. iminoproton resonances from double helical parts in nucleic acid molecules.

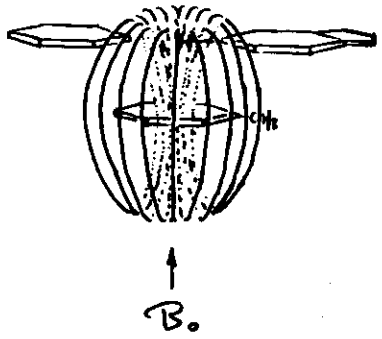

Figure 20

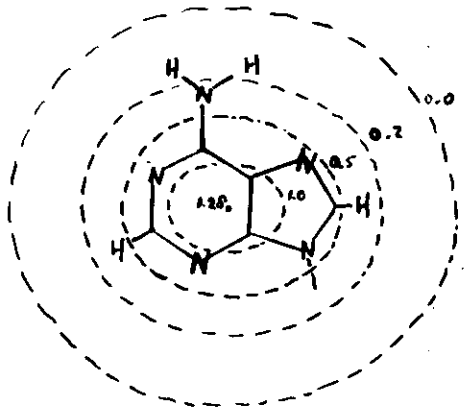

Figure 21 Ring current shielding values due to the ring current in adenine in a plane 3.4 Å from the molecular

Proton resonances of a particular base can be shifted by the ring currents of adjacent basepairs (Fig 20) in double helices. For double helices Tables compiled by Arter and Schmidt (1976) Nucleic Acids Research, 3, 1437, can be employed to calculate resonance positions.

E. SPIN - SPIN COUPLING

( ]- coupling)

The resonance of a particular proton (nucleus) may be split into a doublet or triplet etc. A simple example is presented by the molecule: $CHCl_2 - CH_2Br$

Figure 23

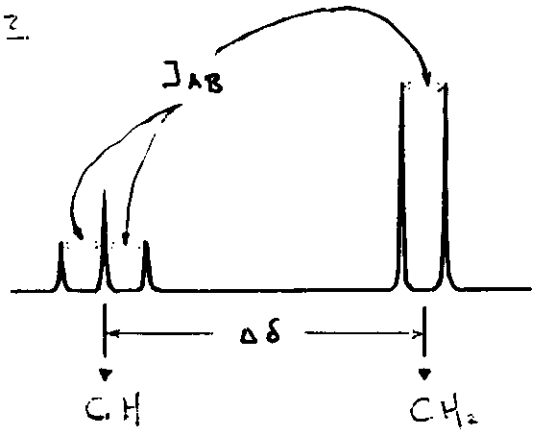

The C-H resonance is a triplet, the CH_2 resonance is a doublet

$\Delta\delta$ is the chemical shift between the C-H and $C-H_2$ resonance positions

J_{AB} is the]- coupling between

37

the CH and $-CH_2$ group. In nucleic acids one finds J-coupling between the H_5 and H_6 protons in cytosine and in uridine, moreover there is J-coupling between the sugar protons (see Fig 13,-15) The doublet splitting of the CH_2 signal of $CHCl_2 - CH_2Br$ arises from the two different orientations (parallel and anti-parallel) the CH spin has in an applied magnetic field This gives rise to two slightly different magnetic fields at the position of the CH_2 group. These fields, which are superimposed on the chemical shift effect, are transferred through the

38

bonding electrons.

Pictorial representation of the mechanism

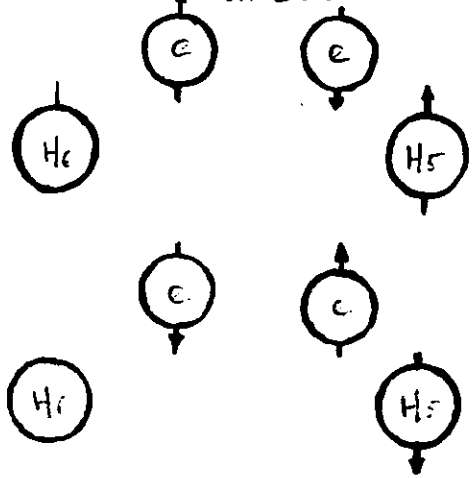

Figure 23

The electron spins are polarized by the spin of the CH group; the CH_2 spins feel the field of the polarized electrons. The latter is different of different spin orientations of the CH group. (These spin orientations are indicated in the spectrum of $CH_2Cl_2 - CHBr_2$)

39

In nucleic acids the vicinal coupling constant between two proton spins on adjacent carbon atoms is of particular interest. This coupling constant contains structural information. The Karplus relation

$$^3J_{HH} = A\cos^2\varphi + B\cos\varphi + C \quad (46)$$

relates the dihedral angle φ to the J-coupling $^3J_{HH}$ (between the two protons).

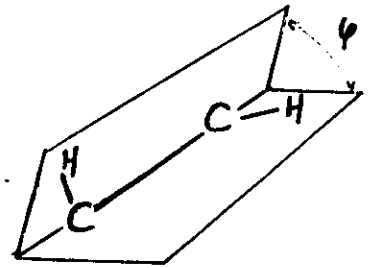

Figure 23

Application of this equation to 315 compounds and comparison

40

of theoretical J-coupling with measured J-couplings yields Fig 24. An improved equation in which substituent effects are included (Haasnoot et al. (1980) Tetrahedron 36, 2783) is:

$$^3J_{HH} = P_1\cos^2\varphi + P_2\cos\varphi + P_3 + \sum \Delta\chi_i\left[P_4 + P_5\cos^2(\xi\varphi + P_6|\Delta\chi_i|)\right] \quad (47)$$

where $\Delta\chi_i$ is the electronegativity of substituent i; ξ is +1 or −1 depending on the orientation of the substituent.

41

Optimum values for the parameters $P_1 - P_6$ were determined (using the 315 compounds mentioned above) with a least squares iterative procedure. Comparison of calculated and experimental J-couplings yields Fig 25. Hence, incorporation of electronegativity effects improves the usefulness for structural determination.

A-type double helices are characterized by N-type (C3' endo) en B-type double helices by S-type (C2'-endo) sugar conformations. Hence, the sugar pucker is an important

42

Figure 24 KARPLUS

$$^3J = A\cos^2\varphi + B\cos\varphi + C$$

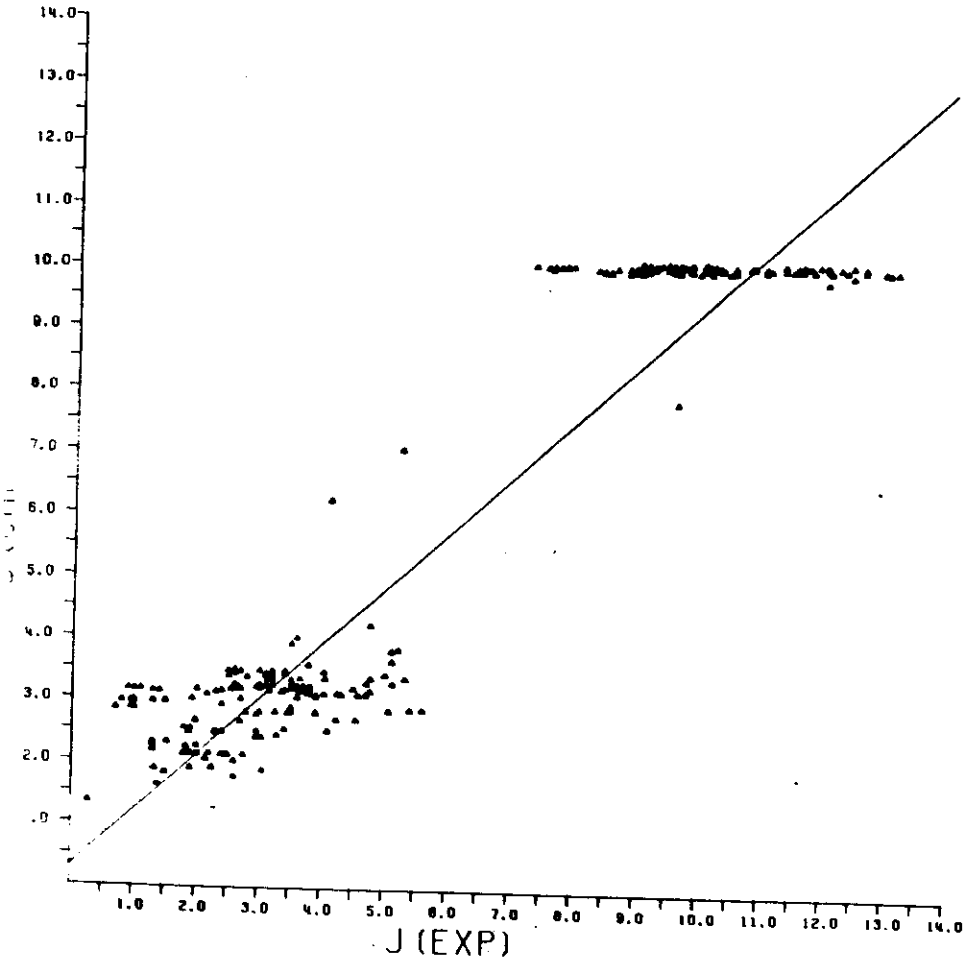

43

Generalized Karplus Equation

$$^3J = P_1 \cos^2\varphi + P_2 \cos\varphi + \Sigma \Delta\chi_i \left(P_4 + P_5 \cos^2(\xi_i \cdot \varphi + P_6 \Delta\chi_i) \right)$$

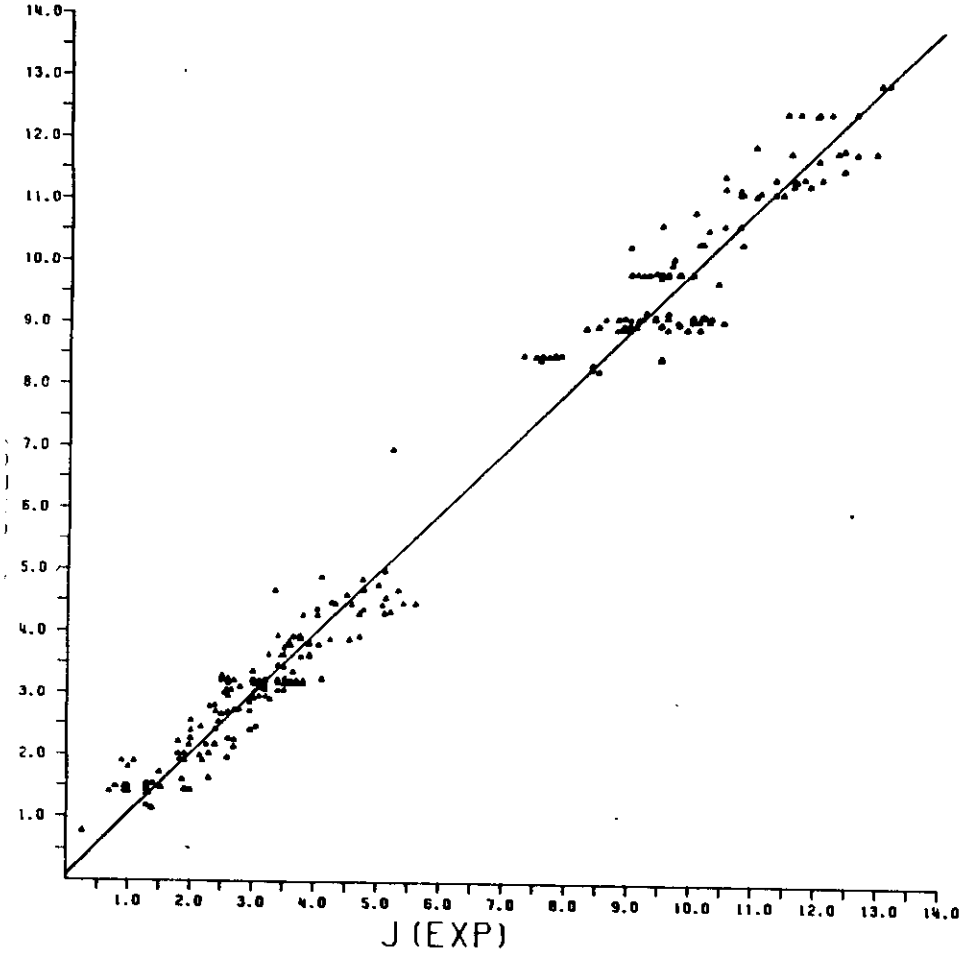

Figure 25

44

probe for * conformational studies of nucleic acids. Combination of the Haasnoot equation (47) with a pseudorotation analysis (Altona, Recl. Trav. Chim. Pays Bas 101, 413 (1982)) shows that for N-type sugar rings $J_{1',2'} \approx 1$ Hz for ribose rings and $J_{1',2'} \approx 1.5 - 3.3$ Hz for deoxy sugars

For S-type sugar rings $J_{1',2'} \approx 7.9$ Hz for ribose rings and $J_{1',2'} \approx 10$ Hz for dexo ribose rings.

A simple relationship for determing the percentage of S- conformation for deoxy sugars was discovered by Altona (see reference above)

Figure 26 -45-

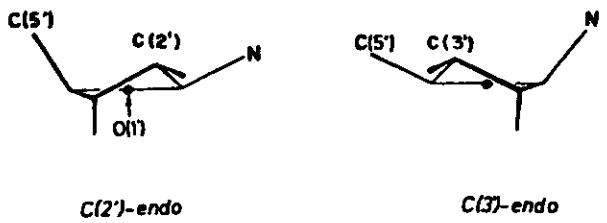

C(2')-endo C(3)-endo

Comparison of C2' endo and C3' endo conformations.

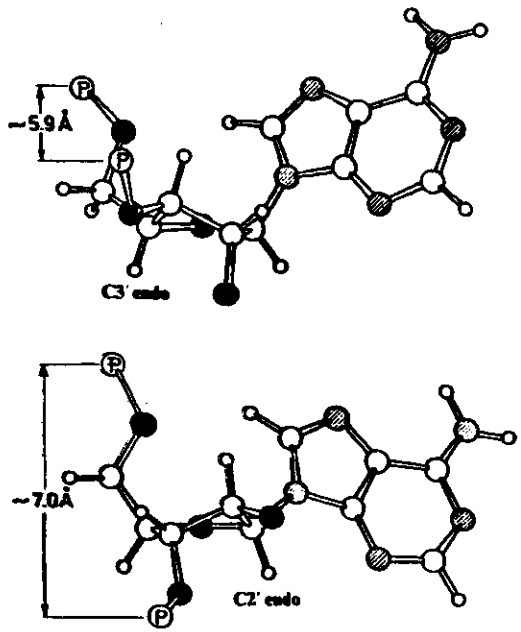

46

$$\% S = (17.8 - \Sigma J_{2'}) / 10.9 \qquad (48)$$

where

$$\Sigma J_{2''} = J_{1',2'} + J_{2'',3'} \qquad (49)$$

Thus, when the spectra are sufficiently resolved the sugar conformation can be deduced from the spectra.

II. THE OVERHAUSER EFFECT

A. Convential 1-dimensional approach.

The Overhauser effect (NOE) is the reduction (or gain) in intensity of one resonance (or groups of resonances) when a different resonance (or group of resonances) is selectively saturated

Figure 27.

Pulse saguence employed to observe NOE's

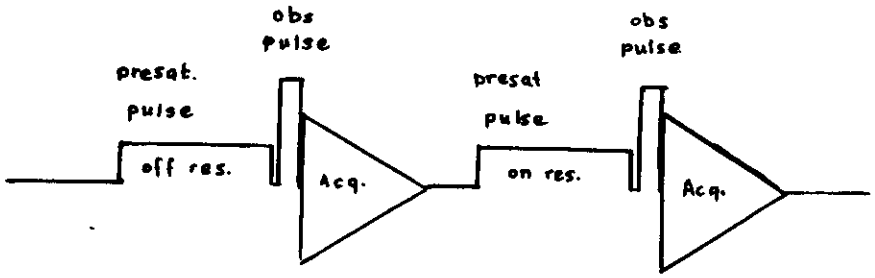

Figure 28

Results for a hypothetical two spin system without J-coupling

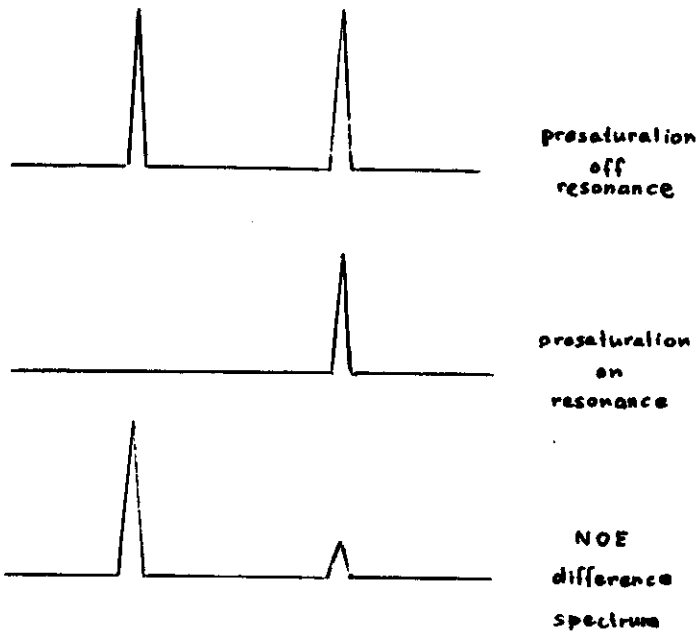

Theory for a two spin system

For a two spin system we have the following energy levels with transition probabilities

W_1^A, W_1^X, W_2, W_0

49

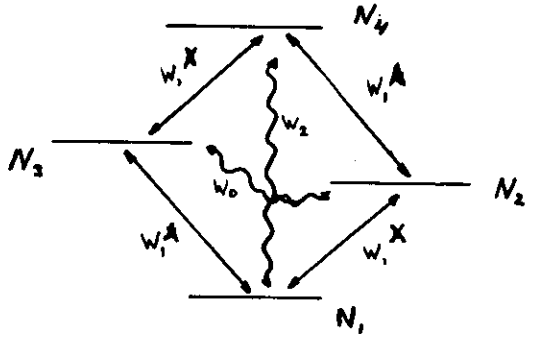

Figure 2g

Energy levels and transition probabilities (for a two-spin (AX) system.

The time dependence of the populations N_1, N_2, N_3 and N_4 are given by the rate equations:

$$\frac{dN_1}{dt} = -\left(W_1^A + W_1^X + W_2\right)\left(N_1 - N_1^\circ\right) + W_{1X}\left(N_2 - N_2^\circ\right) + W_1^X\left(N_3 - N_3^\circ\right) + W_2\left(N_4 - N_4^\circ\right) \quad (50a)$$

$$\frac{dN_2}{dt} = W_1^X\left(N_1 - N_1^\circ\right) - \left(W_1^A + W_1^X + W_0\right)\left(N_2 - N_2^\circ\right) + W_0\left(N_3 - N_3^\circ\right) + W_1^A\left(N_4 - N_4^\circ\right) \quad (50b)$$

$$\frac{dN_3}{dt} = W_1^A\left(N_1 - N_1^\circ\right) + (1\, W_0\left(N_2 - N_2^\circ\right) - \left(W_1^A + W_1^X + W_0\right)\left(N_3 - N_3^\circ\right) + W_1^X\left(N_4 - N_4^\circ\right) \quad (50c)$$

50

$$\frac{dN_4}{dt} = W_2\left(N_1 - N_1^\circ\right) + W_1^A\left(N_2 - N_2^\circ\right) + W_1^X\left(N_3 - N_3^\circ\right) - \left(W_1^A + W_1^X + W_2\right)\left(N_4 - N_4^\circ\right) \quad (50d)$$

The N°'s are equilibrium populations

The differences in populations are related to (measurable) magnetizations (in the z-direction; i.e. along the direction of the magnetic field) by:

$$M_{zA} = \frac{1}{\gamma}\,\frac{1}{2}\,\gamma\hbar\left\{\left(N_1 - N_3\right) + \left(N_2 - N_4\right)\right\} \quad (51a)$$

$$M_{zX} = \frac{1}{2}\,\gamma\hbar\left\{\left(N_1 - N_2\right) + \left(N_3 - N_4\right)\right\} \quad (51b)$$

Forming lineair combinations of Eqns. (50) as dictated by Eqns (51) yields the following time dependence of the magnetizations

$$\frac{dM_{zA}}{dt} = -\rho_A (M_{zA} - M_{zA}^\circ) - \sigma (M_{zx} - M_{zx}^\circ) \quad (52a)$$

$$\frac{dM_{zx}}{dt} = -\sigma (M_{zA} - M_{zA}^\circ) - \rho_x (M_{zx} - M_{zx}^\circ) \quad (52b)$$

with

$$\rho_A = W_0 + 2W_1^A + W_2 \quad (53)$$

$$\rho_x = W_0 + 2W_1^x + W_2 \quad (54)$$

$$\sigma = W_2 - W_0 \quad (55) \quad \text{cross relaxation}$$

The general solution to the coupled differential equations (52) is

$$M_{zA} - M_{zA}^\circ = C_{1A} e^{-\lambda_1 t} + C_{2A} e^{-\lambda_2 t} \quad (55a)$$

$$M_{zx} - M_{zx}^\circ = C_{1x} e^{-\lambda_1 t} + C_{2x} e^{-\lambda_2 t} \quad (55b)$$

with

$$\lambda_{1,2} = \frac{(\rho_A + \rho_x) \pm \left\{ (\rho_A - \rho_x)^2 + 4\sigma^2 \right\}^{1/2}}{2}$$

$$= \alpha \pm \mathcal{D} \quad (56)$$

where

$$\alpha = \tfrac{1}{2} (\rho_A + \rho_x) \quad (57)$$

$$\mathcal{D} = \left(\beta^2 + \sigma^2 \right)^{1/2} \quad (58)$$

so that

$$\beta = \tfrac{1}{2} (\rho_A - \rho_x) \quad (59)$$

The constants C are given by

$$C_{1A} = -\frac{1}{2\mathcal{D}} \left\{ -(\beta + \mathcal{D})(M_{zA}(0) - M_A^\circ) - \sigma (M_{zx}(0) - M_x^\circ) \right\} \quad (60a)$$

$$C_{2A} = -\frac{1}{2\mathcal{D}} \left\{ (\beta - \mathcal{D})(M_{zA}(0) - M_A^\circ) + \sigma (M_{zx}(0) - M_x^\circ) \right\} \quad (60b)$$

$$C_{1x} = -\frac{1}{2\mathcal{D}} \left\{ -\sigma (M_{zA}(0) - M_A^\circ) + (\beta - \mathcal{D})(M_{zx}(0) - M_x^\circ) \right\} \quad (60c)$$

$$C_{2x} = -\frac{1}{2\mathcal{D}} \left\{ \sigma (M_{zA}(0) - M_A^\circ) - (\beta + \mathcal{D})(M_{zx}(0) - M_x^\circ) \right\} \quad (60d)$$

The $M_z(0)$ are the magnetizations at time zero and therefore depend on the initial conditions of the experiments.

53

TRANSITION PROBABILITIES

Relaxation in spin systems is caused by fluctuating magnetic and/or electric fields at the sites of the observed nuclei. These fluctuating field results from the thermal motion of atoms and molecules in matter. When the fluctuations have the proper frequency characteristics they may ~~induce~~ give rise to transitions between the spin energy levels. Assuming that dipole - dipole relaxation is the dominating relaxation ~~mech~~ mechanism in the AX spin system, the transition probabilities can be calculated

54

$$W_{1A} = \frac{3}{20} \frac{\gamma_A^2 \gamma_X^2 \hbar^2}{r^6} \frac{\tau_c}{1 + \omega_A^2 \tau_c^2} \quad (61)$$

$$W_{1X} = \frac{3}{20} \frac{\gamma_A^2 \gamma_X^2 \hbar^2}{r^6} \frac{\tau_c}{1 + \omega_X^2 \tau_c^2} \quad (62)$$

$$W_0 = \frac{1}{10} \frac{\gamma_A^2 \gamma_X^2 \hbar^2}{r^6} \frac{\tau_c}{1 + (\omega_A - \omega_X)^2 \tau_c^2} \quad (63)$$

$$W_2 = \frac{3}{5} \frac{\gamma_A^2 \gamma_X^2 \hbar^2}{r^6} \frac{\tau_c}{1 + (\omega_A + \omega_X)^2 \tau_c^2} \quad (64)$$

Where τ_c is the rotational correlation time (a measure for the rate of tumbling of the molecules); ω_A and ω_X are the Larmor precession frequencies of the A and X spins respectively. All transition probabilities are proportional to r^{-6}, where r is the distance between spins A and X.

LIMIT OF EXTREME NARROWING

Tumbling of molecules is fast (small molecules) : $\omega_A \tau_c \ll 1$; $\omega_X \tau_c \ll 1$ so that

$$W_1 = W_{1A} = W_{1X} = \frac{3}{20} \frac{\gamma_A^2 \gamma_X^2 \hbar^2}{r^6} \tau_c \qquad (65)$$

$$W_0 = \frac{1}{10} \frac{\gamma_A^2 \gamma_X^2 \hbar^2}{r^6} \tau_c \qquad (66)$$

$$W_2 = \frac{3}{5} \frac{\gamma_A^2 \gamma_X^2}{r^6} \tau_c \qquad (67)$$

The transition probabilities are directly proportional to τ_c :

$$W_0 : W_1 : W_2 = 2 : 3 : 12 \qquad (68)$$

LIMIT OF SLOW TUMBLING

Tumbling of molecules is slow (large molecules : proteins, nucleic acids) $\omega_A \tau_c \gg 1$; $\omega_X \tau_c \gg 1$ so that

$$W_{1A} = \frac{3}{20} \frac{\gamma_A^2 \gamma_X^2 \hbar}{r^6} \frac{1}{\omega_A^2 \tau_c} \qquad (69)$$

56

$$W_{1X} = \frac{3}{20} \frac{\gamma_A^2 \gamma_X^2 \hbar^2}{r^6} \frac{1}{\omega_X^2 \tau_c} \qquad (70)$$

$$W_0 = \frac{1}{10} \frac{\gamma_A^2 \gamma_X^2 \hbar^2}{r6} \frac{1}{(\omega_A - \omega_X)^2 \tau_c} \qquad (71)$$

$$W_2 = \frac{3}{5} \frac{\gamma_A^2 \gamma_X^2 \hbar^2}{r6} \frac{1}{(\omega_A + \omega_X)^2 \tau_c} \qquad (72)$$

With increasing τ_c's the transition probabilities decrease ; this means the relaxation times become longer.

"LIKE" SPINS

Spins A and X have the same Larmor frequencies e.g. A and X are both protons . The equations simplify :

$$W_1 = W_{1A} = W_{1X} = \frac{3}{20} \frac{\gamma^4 \hbar^2}{r^6} \frac{\tau_c}{1 + \omega^2 \tau_c^2} \qquad (73)$$

$$W_0 = \frac{1}{10} \frac{\gamma^4 \hbar^2}{r^6} \tau_c \qquad (74)$$

57

$$W_2 = \frac{3}{5} \frac{\gamma^4 \hbar^2}{r^6} \frac{\tau_c}{1 + 4\omega^2 \tau_c^2} \qquad (15)$$

As expected, for extreme narrowing again $W_0 : W_1 : W_2 = 2 : 3 : 12$ as for the general situation (including unlike spins). An interesting difference shows up in the slow tumbling limit: W_0 increases with increasing τ_c in contrast to the other transition probabilities and in contrast to the situation with unlike spins. This is important; shortly we shall see that this gives rise to spin diffusion in more general situations (larger spin systems).

58

THE STEADY STATE OVERHAUSER EFFECT

Return to Eq. 52a

$$\frac{dM_{zA}}{dt} = -\rho_A (M_{zA} - M_A^\circ) - \sigma (M_{zx} - M_x^\circ)$$

When the X-spin system is continuously saturated; i.e $M_x = 0$, a steady state for the spin system is obtained. Hence:

$$0 = -\rho_A (M_{zA} - M_A^\circ) + \sigma M_x^\circ \qquad (76)$$

or

$$M_{zA} = M_A^\circ + \frac{\sigma}{\rho_A} M_x^\circ \qquad (77)$$

Thus, in these steady state conditions M_{zA} is not equal to the equilibrium magnetization, M_A°. The magnetization of the A-spins increases or decreases with an amount $\frac{\sigma}{\rho_A} M_x^\circ$ as a

result of the continuous irradiation of the X-spins. This is the Overhauser effect § which in the literature is defined as:

$$NOE = 1 + \eta \qquad (70)$$

where

$$\eta = \frac{M_{zA} - M_A^\circ}{M_A^\circ} = \frac{\sigma}{\rho_A}\frac{M_X^\circ}{M_A^\circ} = \frac{\sigma}{\rho_A}\frac{\gamma_X}{\gamma_A} \qquad (71)$$

is the enhancement factor;

NOE stands for nuclear Overhauser effect. The sign and magnitude of η depend on the sign and magnitude of γ_X/γ_A as well as the sign and magnitude of σ/ρ_A

60

Examples of the influence of γ_X/γ_A (assume γ_X is magnetic gyric ratio of protons)

Nucleus	γ_A	γ_X/γ_A
^1H	26753	1
^{13}C	6728	3.97
^{15}N	-2712	-9.86
^{31}P	10840	2.46

When protons are saturated the factor γ_X/γ_A contributes to an increase of ^{13}C, and ^{31}P magnetization if the sign of σ/ρ_A is positive, on the other hand for ^{15}N the magnetization is decreased when the sign of σ/ρ_A is positive.

61

THE FACTOR σ/ρ_A

According to eqns. (53) and (55)

$$\sigma/\rho_A = \frac{W_2 - W_0}{W_0 + 2W_1^A + W_2} \qquad (19)$$

Note that the factor $\frac{\gamma_A^2 \gamma_X^2 \hbar^2}{r^6}$

cancels out of this expression, hence the steady state NOE (in contrast to the time dependent NOE) does not depend on the distance between the spins. In the fast tumbling limit $\sigma/\rho_A = 1/2$ (see eqns. 69-73) hence in this limit the enhancement factor $\eta = \gamma_X/2\gamma_A$, which does not depend on τ_c.

Calculated examples:

AX	H···H	^{13}C··H	^{15}N··H	^{31}P···H
η	1/2	2	−5	1.23

62

Also for the slow tumbling limit η does not depend on τ_c

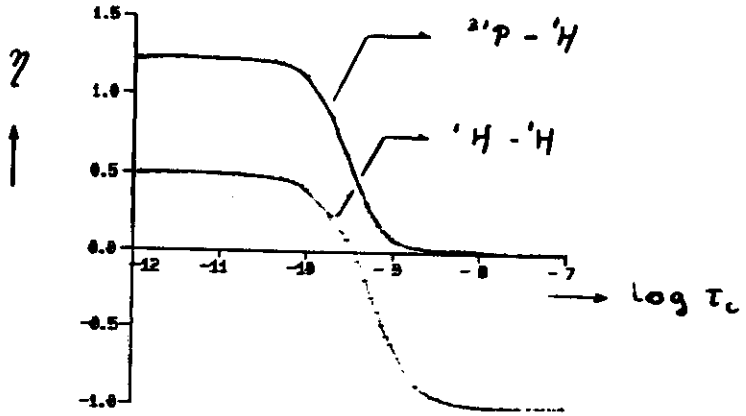

Calculations of Overhauser effects at 500 MHz as a function of τ_c. The Overhauser effects were calculated for a ^{31}P - ^{1}H spin pair — the proton is saturated and the NOE is observed for ^{31}P — and for a ^{1}H - ^{1}H spin pair — one proton is saturated the NOE for the other

proton is observed. Note that for short and long correlation times η does not depend on τ_c. The proton-proton NOE varies from $+1/2$ for short correlation times to -1 for longer correlation times (i.e. for molecules with molecular weights of about 5000 daltons or higher). For $W_2 - W_0 = 0$, $\eta = 0$.

The $^{31}P-H$ NOE varies from 1.23 for short correlation times to zero for longer correlation times. Hence, for an important class of nucleic acids (MW $\geq$ 5000) no phosphorous proton NOE's can be observed.

MULTIPLE SPIN SYSTEMS

The equations of motion describing the time dependence of the magnetization of the two spin system (Eqns 52) can be generalized to multiple spin systems; if interactions between spins is pairwise so that

$$\frac{dM_{zi}}{dt} = -R_i\{M_{zi} - M_i^\circ\} - \sum_{j\neq i}\sigma_{ij}\{M_{zj} - M_j^\circ\} \qquad (80)$$

with

$$R_i = \sum_{j\neq i}\left(W_{0ij} + 2W_{ij} + W_{2ij}\right) \qquad (81)$$

and

$$\sigma_{ij} = W_{2ij} - W_{0ij} \qquad (82)$$

For a total of N spins there are N coupled differential equations to be solved. In the conventional 1D-Overhauser experiment one resonance, k, is saturated with a selective saturation pulse.

For simplicity we assume that saturation occurs instantaneously at the start of the saturation pulse. Then the time dependence of the magnetization of spins i during the saturation pulse is:

$$\frac{dM_{zi}}{dt} = R_i\{M_{zi} - M_i^\circ\} - \sum_{\substack{j\neq i \\ j\neq k}} \{M_{zj} - M_j^\circ\} - \sigma_{ik} M_k^\circ \qquad (83)$$

This equation can be rewritten to describe the time dependence of the Overhauser effect

$$\frac{d\eta_i}{dt} = -R_i\eta_i - \sum_{j\neq i,k} \sigma_{ij}\eta_j - \sigma_{ik} \qquad (84)$$

with

$$\eta_i = \frac{M_{zi} - M_i^\circ}{M_i^\circ} \qquad (85)$$

(it is assumed that all M_i° are equal)

The set of coupled differential equations can be cast into a matrix equation:

$$\frac{d}{dt}\underset{\sim}{\eta} = -\underset{\sim}{W}\underset{\sim}{\eta} - \underset{\sim}{\sigma} \qquad (86)$$

A formal solution to this equation is:

$$\underset{\sim}{\eta} = \underset{\sim}{\sigma} \cdot \underset{\sim}{W}^{-1} \left(\underset{\sim}{1} - e^{-\underset{\sim}{W} t} \right) \qquad (87)$$

Written as a series expansion:

$$\underset{\sim}{\eta} = \underset{\sim}{\sigma} \cdot \underset{\sim}{W}^{-1} \left[\underset{\sim}{1} - \underset{\sim}{1} + \underset{\sim}{W} t - \frac{1}{2!} \underset{\sim}{W} \cdot \underset{\sim}{W} t^2 + \frac{1}{3!} \underset{\sim}{W} \cdot \underset{\sim}{W} \cdot \underset{\sim}{W} t^3 - \ldots \right]$$

$$= \underset{\sim}{\sigma} t - \frac{1}{2!} \underset{\sim}{W} t^2 + \frac{1}{3!} \underset{\sim}{\sigma} \cdot \underset{\sim}{W} \cdot \underset{\sim}{W} t^3 - \ldots \qquad (88)$$

From this equations the time dependence of the magnetization of individual spin types can be extracted; for spins i follows

$$\eta_i = \sigma_{ik} t - \frac{1}{2} \sum_{j \neq i,k} \sigma_{ij} \sigma_{jk} t^2 - \frac{1}{2} R_i \sigma_{ik} t^2 + \frac{1}{6} R_i \sigma_{ik} t^3 + \frac{1}{6} \sum_{l \neq i,j,k} \sum_{j \neq i,l} \sigma_{ij} \sigma_{jl} \sigma_{lk} t^3 + \frac{1}{6} \sum_{j \neq i,k} R_i \sigma_{ij} \sigma_{jk} t^3$$

$$+ \frac{1}{6} \sum_{j=i,k} R_j \sigma_{ik} \sigma_{jk} t^3 \qquad (89)$$

The first term of the r.h.s of the equation is responsible for the first order Overhauser effect; the saturation (magnetization) of spins k is transferred, by means of the cross relaxation σ_{ik}, to spins i. The second term on the r.h.s of the equation represents a so called second order Overhauser effect After saturation of spins k magnetization is transfened to spin i but now mediated via spins j..

The magnetization transfer can be schematized as follows:

Figure 31

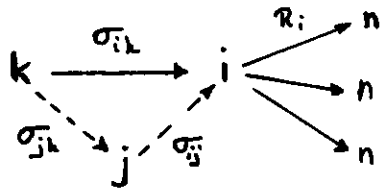

In absence of mediated cross relaxation (i.e. in absence of higher order Overhauser effects) a closed analytical expression can be obtained even for a multiple spin system:

$$\eta_i = \frac{\sigma_{ik}}{R_i}\left(1 - e^{-R_i t}\right) \qquad (90)$$

In general for sufficiently short presaturation pulses:

$$\eta_i = \sigma_{ik}\, t \qquad (91)$$

Hence, the NOE becomes proportional to the length of the saturation pulse and to the cross relaxation rate σ_{ik}.

For large molecules (e.g. molecules with molecular weights $\geq$ 5000 dalton and Larmor precession frequencies ~ 500 MHz)

$$\sigma_{ik} = -\frac{\gamma^4 \hbar^2}{10\, r_{ik}^6}\, \tau_c \qquad (92)$$

Thus for proper experimental conditions the Overhauser effect is proportional to r_{ik}^{-6} and in principle this effect can be employed to measure the distance between nuclei in molecules (in practice some problems are encountered)

APPLICATION OF THE OVERHAUSER EFFECT

Example : the assignment of the iminoprotons of yeast $tRNA^{Phe}$ (Heerschap et al. Nucleic Acids Research 10, 6901 (1982); ibid 11, 4403 (1983); ibid 11, 4501 (1983); Roy, S. and Redfield A.G. Biochemistry 22, 1306 (1983))

Transfer RNA's consist of chains of about 75 nucleotides The distributions of the bases in these chains is such that, via base pairing, a characteristic cloverleaf structure can be formed with (or double helical regions (see Fig).

Subsequently, from the "cloverleaf" a three dimensional structure can be folded as shown in Fig (32). The different parts of the molecule are indicated.

In NMR studies the iminoprotons have played an important role. Their resonances can only be observed for tRNA dissolved in H_2O (instead of D_2O) because of the exchange properties of the iminoproton: (vide infra). For a 1mM solution of tRNA the H_2O

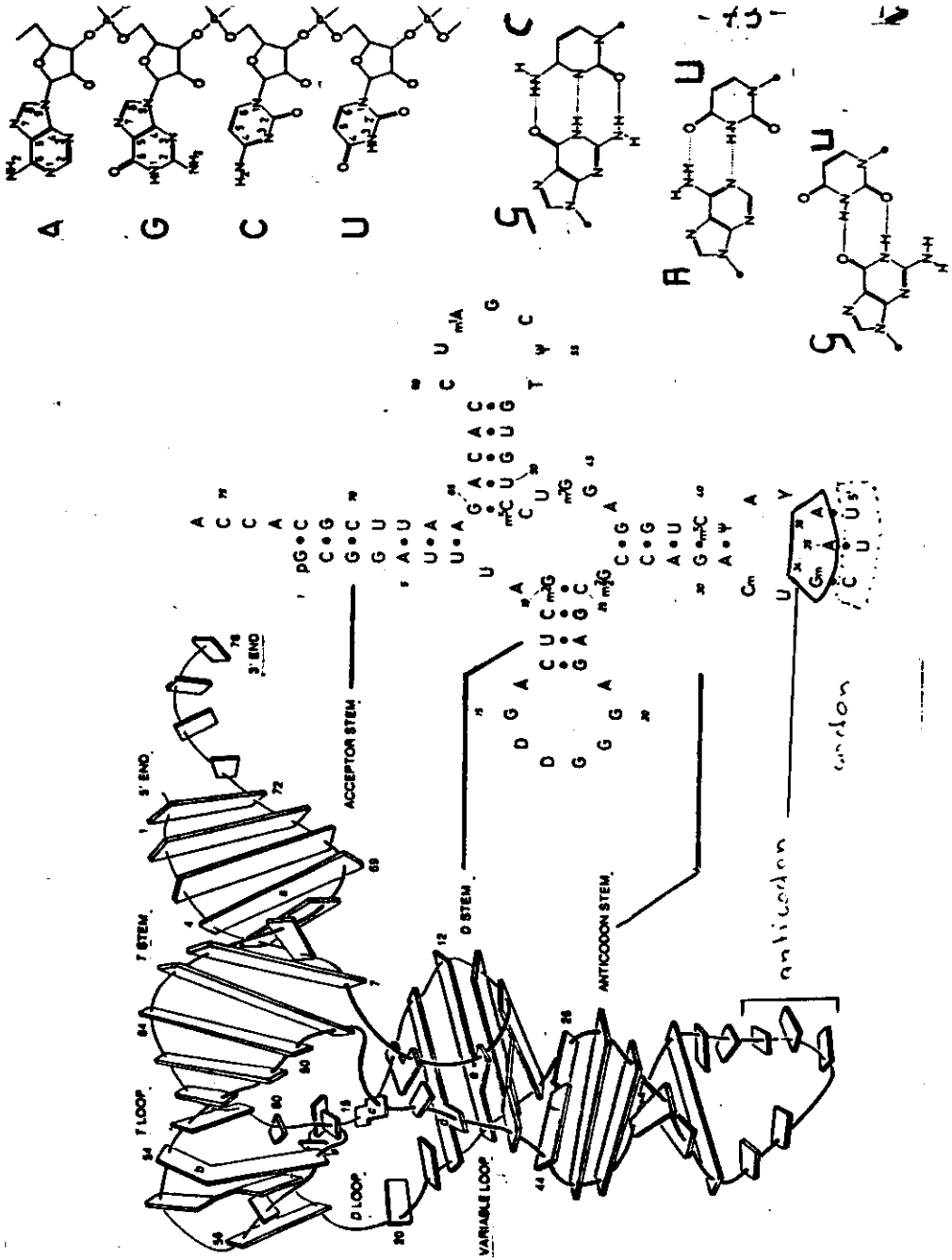

Figure 32

signal is about 100.000 times more intense than the imino proton signals. This present a dynamic range problem to the NMR computer. Therefore the water signal is suppressed by employing a semi selective observation pulse (which avoids excitation of the water spins as much as possible) in combination with alternate delayed acquisition. (Haasnoot and Hilbers, Biopolymers 22 1259 (1983)). In this way a spectrum of yeast $tRNA^{Phe}$ can be obtained as presented in Fig 33. The positions of the different proton resonances is indicated.

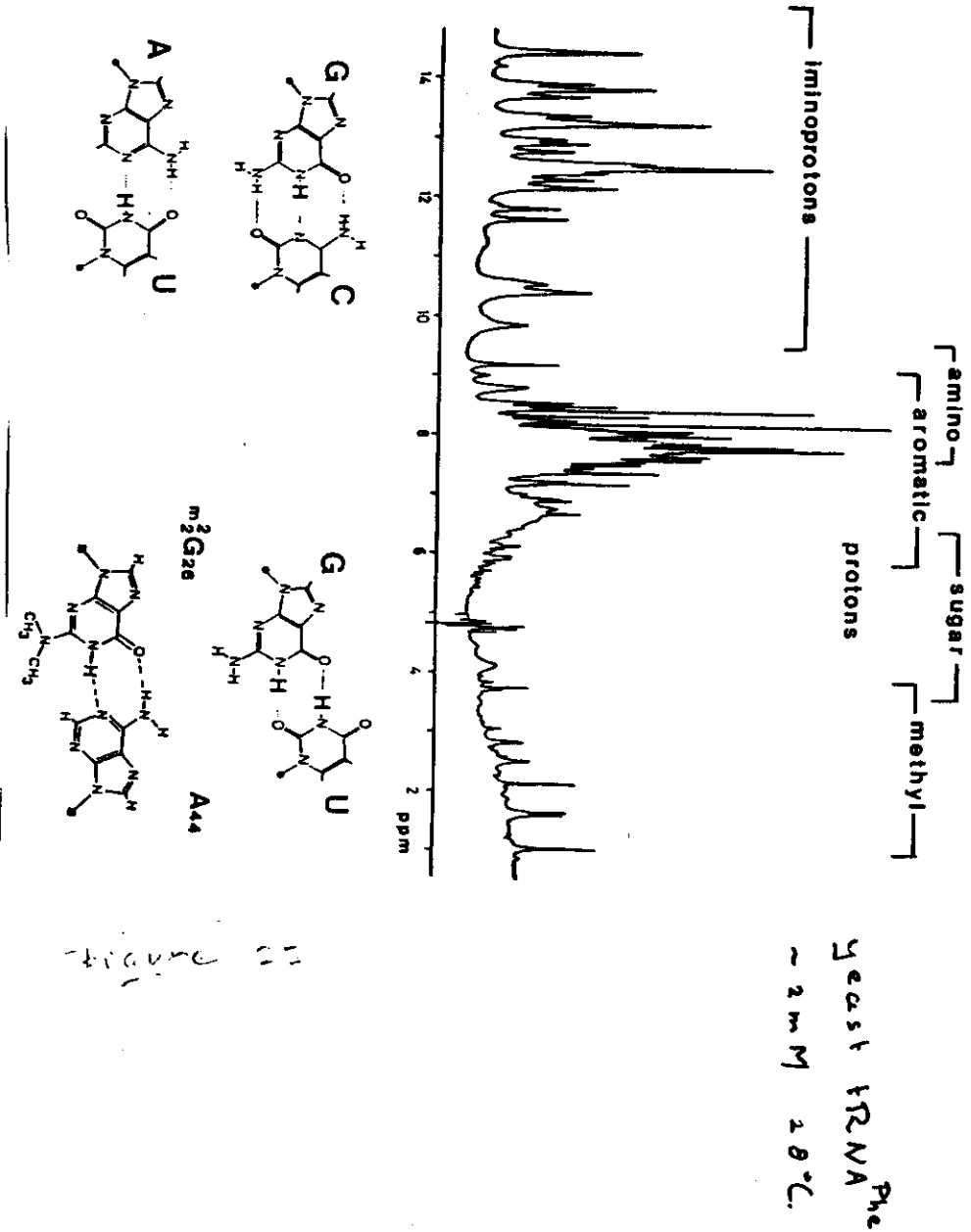

Figure 22

least $tRNA^{Phe}$
~ 2 mM
20°C.

In double helical regions the distance between the imino protons of adjacent basepairs varies between 3.5 and 5 Å. One then expects to measure Over hauser enhancements of 1 - 10 %.

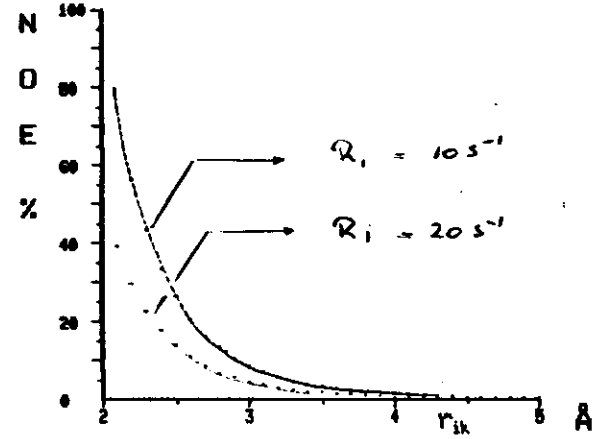

Figure 23. Enhancements calculated with Eq. 22

$$\eta_i = \frac{\sigma_{ik}}{R_i}\left(1 - e^{-R_i t}\right)$$

as a function of the distance between spins i and k.

$\tau_c = 3 \times 10^{-9}$ s, $t = 0.3$ s.

These effects may be employed for sequential assignments of the iminoproton resonances. To start such an identification to have an unambiguously assigned resonance available as a starting point. The iminoprotons of the GU pair in the acceptor stem (see Fig 32) may serve this purpose because they are only 2.4 Å apart from each other and expected to give rise to nOE's of ~ 20 % (Fig 34) In yeast $tRNA^{Phe}$ it is the only pair of iminoprotons giving rise to an effect of this size This is exemplified in Fig 35

Figure 35 Overhauser effects between iminoprotons in GU pair.

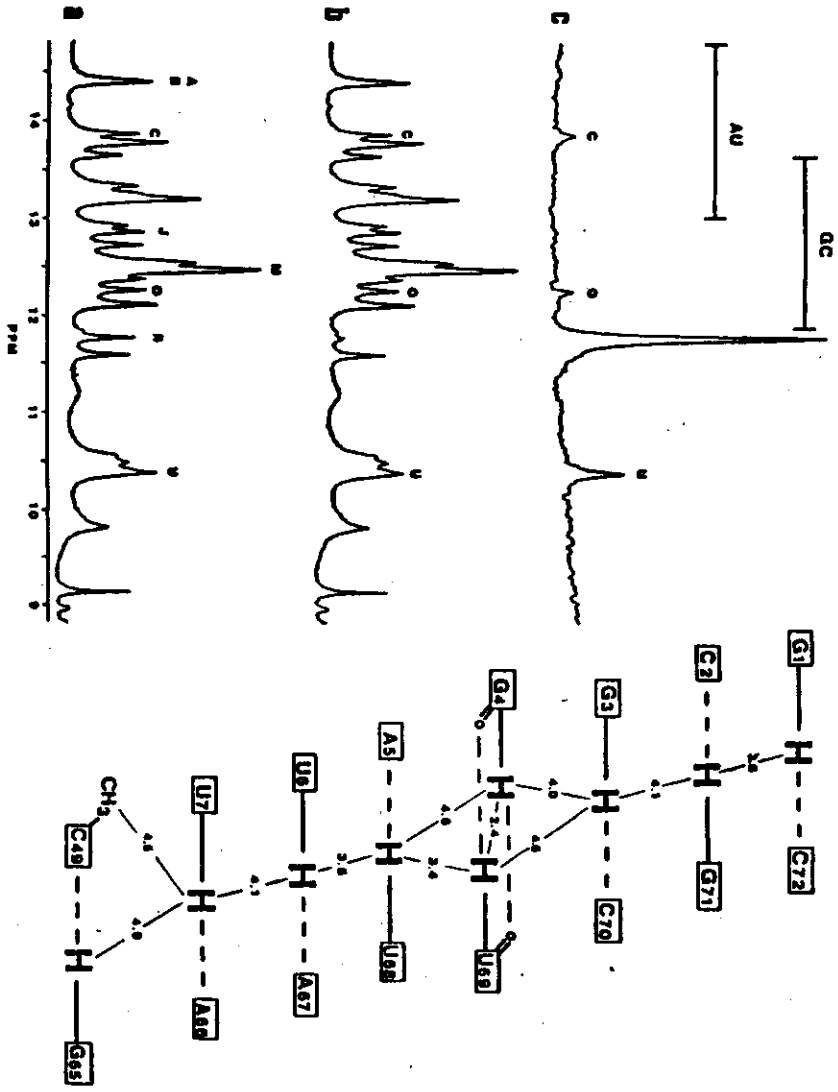

In Fig (35) spectrum (a) is the unperturbed iminoproton spectrum; in spectrum (b) resonance R is saturated; spectrum (c) is the NOE difference spectrum obtained by subtracting (b) from (a) (The pulse sequence and procedure outlined in Fig 27 and 28 was used. The imino protonpair of the GU pair gives rise to the largest NOE in the iminoproton spectrum (resonances R and U) The NOE's measured at the positions of resonances C and O show that these latter two resonances can be assigned to basepair A_5-U60 and G_3-C_{70} respectively. These resonances serve as new starting points for

the assignment of the resonances of the next set of neighbours. and so on. In the way an "NOE walk" is performed through the molecule. Difficulties one may encounter in such a procedure will be discussed.

A summary of the assignments is given in Fig 36. Note that all secondary as well as tertiary iminoprotons are assigned

Conclusions from the NOE studies and assignments.

a) All iminoproton resonances expected on the basis

Fig. 36

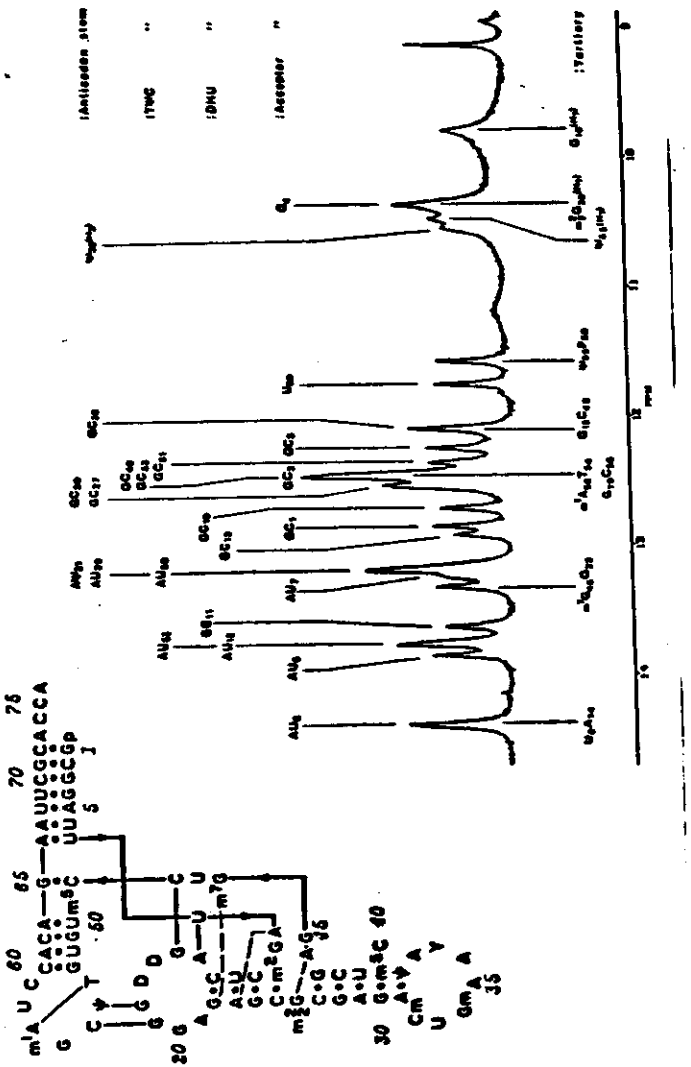

of the 3 dimensional structure are present in the spectrum

b) the acceptor stem is stacked upon the T-stem

c) the D-stem is stacked upon the anticodon stem with G 26 A 44 in between.

Thus the NOE experiments indicate that the most outstanding feature of the tRNA structure namely its L-form is present in solution.

As follows from Fig 37 this is true for different solution conditions (in particular with and without Mg^{2+} ions).

NOE's can also be used to determine binding sites of spermidine on tRNA (see Fig 38)

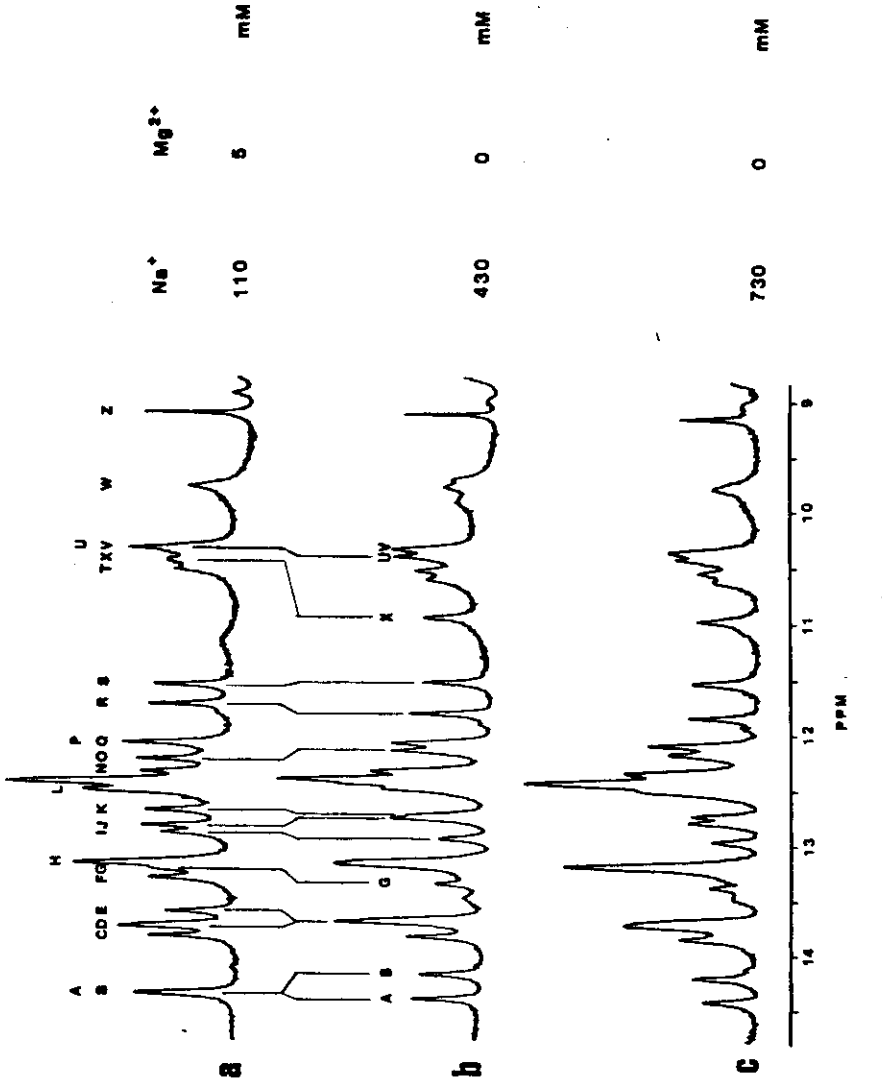

Figure 37 : Imino spectrum under different salt conditions

Figure 38

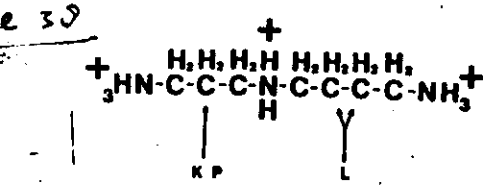

T = 23°C,
110 mM Na^+,
1.0 mM Mg^{++} (var),
Spermidine : tRNA = 1:1

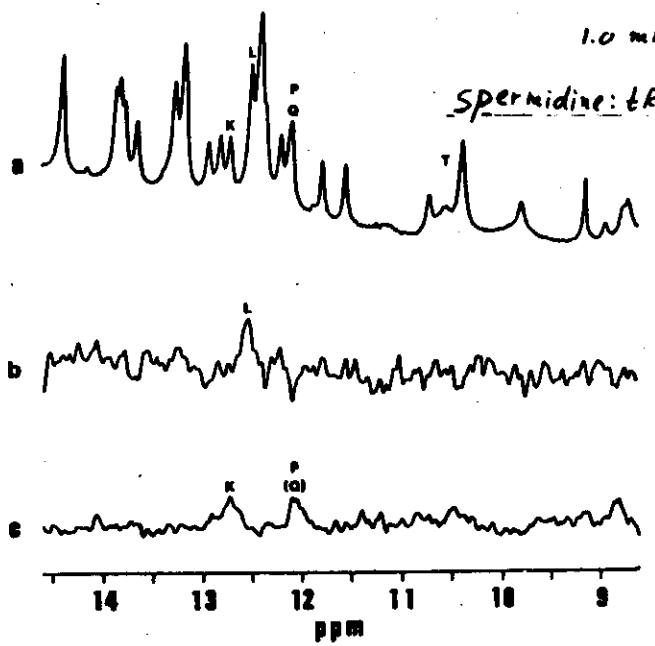

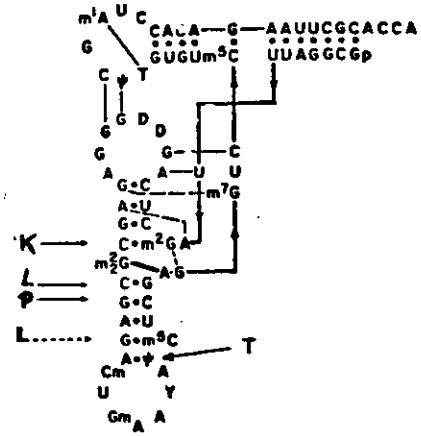

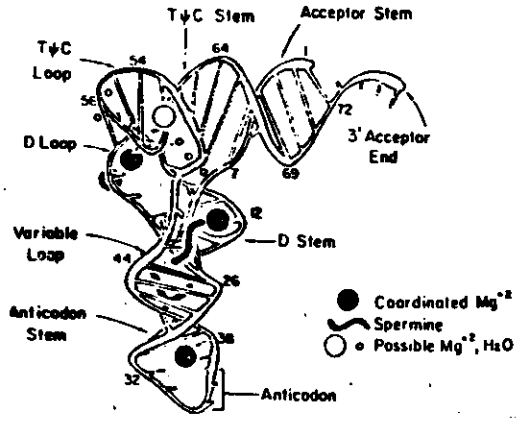

III THE TWO DIMENSIONAL OVERHAUSER EFFECT

Two dimensional (2D) spectra have two frequency axes. The signals, $S(\omega_1, \omega_2)$, observed in such a spectrum, are a function of two independent frequency variables ω_1 and ω_2. The spectrum is obtained after a two dimensional Fourier transformation of a function $s(t_1, t_2)$ that depends on two independent time variables t_1 and t_2.

To obtain a two dimensional NOE spectrum the following pulse sequence is used:

Figure 3g

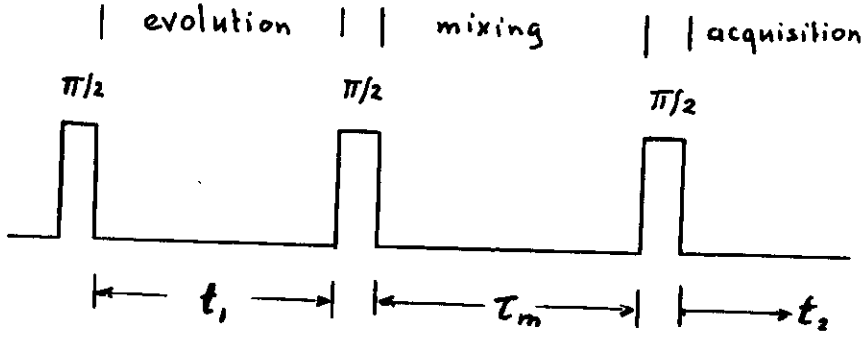

The effect of these three pulses on a two spin system with spins A an B is shown below

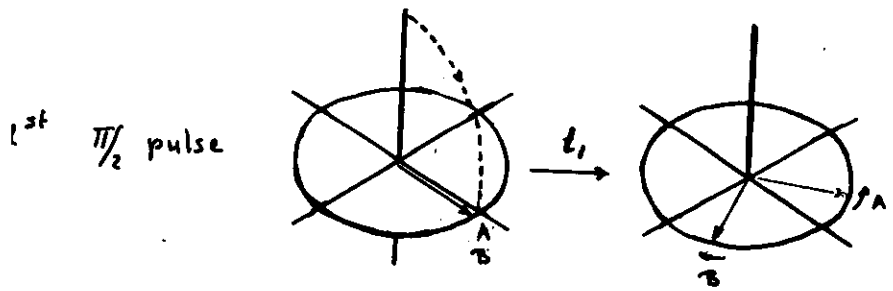

The first $\pi/2$ pulse turns the magnetization of the A and B

spins parallel to the y-direction. During the evolution period, t_1, the A and B magnetization rotate each with their respective Larmor frequency around the z-axis and are frequency labelled.

2^{nd} $\pi/2$ pulse

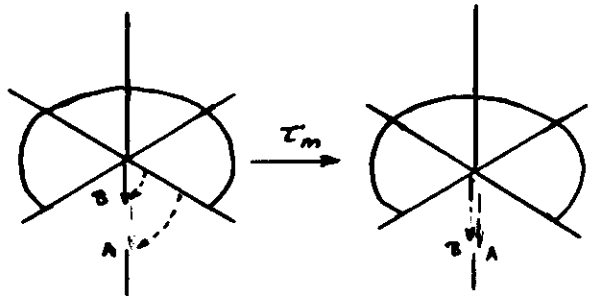

The second $\pi/2$ pulse turns the projections of the A and B magnetizations along the y-direction parallel to the z-axis. During the mixing period, τ_m, A-magnetization is transferred to B-magnetization and vice versa.

As indicated by the arrows the earlier precession frequency is "remembered" after the transfer and eventually gives rise to cross peaks (vide infra).

3^{rd} $\pi/2$ pulse

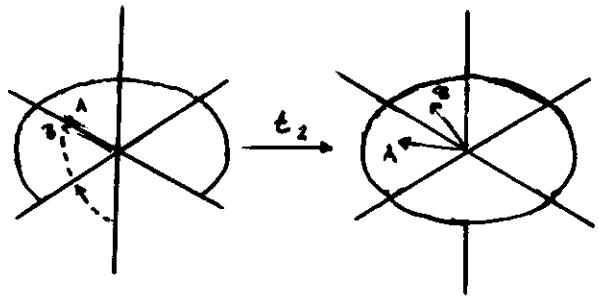

The third (observation) pulse turns the magnetization back to the xy-plane. During the time t_2 the free induction decay is acquired. This process is repeated for different values of t_1 so that we obtain the following information

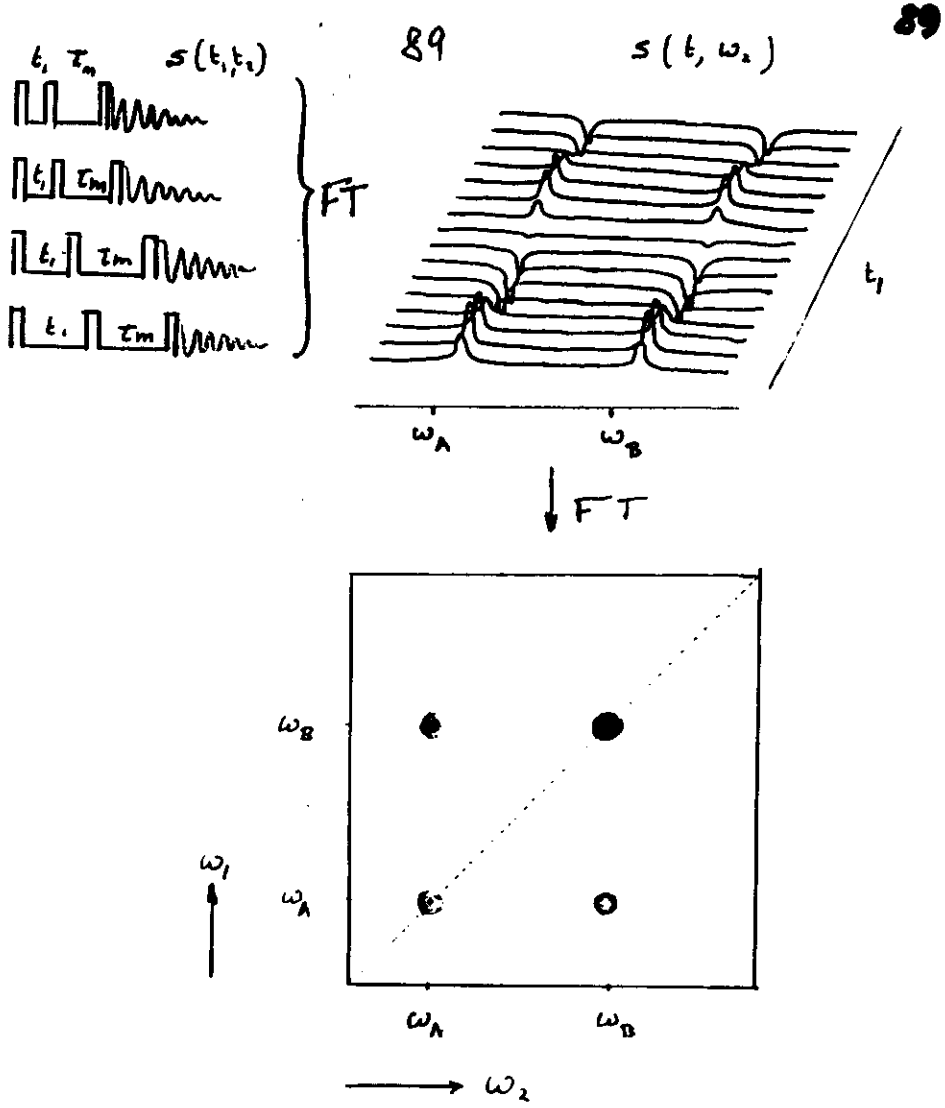

Figure 90

DEVELOPMENT OF THE MAGNETIZATION UNDER INFLUENCE OF A THREE PULSE SEQUENCE.

Consider two different spins A and B with Larmor frequencies ω_A and ω_B. After the first 90° pulse (Figure) the magnetization of A and B start to precess in the x y plane around the z-axis. After a period t_1, their phases will be different from each other due to their different Larmor frequencies :

$$M_A(t_1) = M_A^\circ e^{i\omega_A t_1} e^{-t_1/T_{2A}} \quad (93)$$

$$M_B(t_1) = M_B^\circ e^{i\omega_B t_1} e^{-t_1/T_{2B}} \quad (94)$$

The second 90° pulse turns part of the xy magnetization along the z-axis (we disregard the magnetization remaining in the xy plane)

$$M_z^A = M_A^\circ \cos\omega_A t_1 \, e^{-t_1/T_{2A}} \quad (95)$$

$$M_z^B = M_B^\circ \cos\omega_B t_1 \, e^{-t_1/T_{2B}} \quad (96)$$

Thus at this point the magnetization amplitude depends on t_1.

As a result of dipolar relaxation (or chemical exchange) there is exchange of magnetization, during the mixing time, τ_m.

The effect can be calculated by application of Equations (55)

We assume that $\rho_A = \rho_B = \rho$

At the end of the mixing period

$$M_{zA} - M_A^\circ = -a_{AA}\left\{1 + \cos\omega_A t_1 \, e^{-t_1/T_{2A}}\right\} M_A^\circ - a_{AB}\left\{1 + \cos\omega_B t_1 \, e^{-t_1/T_{2B}}\right\} M_B^\circ \quad (97)$$

and

$$M_{zB} - M_B^\circ = -a_{BB}\left\{1 + \cos\omega_B t_1 \, e^{-t_1/T_{2B}}\right\} M_B^\circ - a_{BA}\left\{1 + \cos\omega_A t_1 \, e^{-t_1/T_{2A}}\right\} M_A^\circ \quad (98)$$

with

$$a_{AA} = \tfrac{1}{2}\left(e^{-(\rho+\sigma)\tau_m} + e^{-(\rho-\sigma)\tau_m}\right) \quad (99)$$

$$a_{BB} = \tfrac{1}{2}\left(e^{-(\rho+\sigma)\tau_m} + e^{-(\rho-\sigma)\tau_m}\right) \quad (100)$$

$$a_{AB} = a_{BA} = \tfrac{1}{2}\left(e^{-(\rho+\sigma)\tau_m} - e^{-(\rho-\sigma)\tau_m}\right) \quad (101)$$

Note that mixing has occurred. After the third pulse, during the acquisition period

$$M_{zA} = \left[-a_{AA}\left(1 + \cos\omega_A t_1 \, e^{-t_1/T_{2A}}\right) M_A^\circ - a_{AB}\left(1 + \cos\omega_B t_1 \, e^{-t_1/T_{2B}}\right) M_B^\circ + M_A^\circ\right] \times \cos\omega_A t_2 \, e^{-t_2/T_{2A}} \quad (102)$$

93

$$M_{zB} = \left[-a_{BB}\left(1 + \cos\omega_B t_1 \, e^{-t_1/T_{2B}}\right) M_B^\circ \right.$$
$$\left. -a_{BA}\left(1 + \cos\omega_A t_1 \, e^{-t_1/T_{2A}}\right) M_A^\circ - M_B^\circ \right] \times$$
$$\cos\omega_B t_2 \, e^{-t_2/T_{2A}}$$

(103)

Consider the magnetization of spins A. In working out equation we shall disregard those terms that do not depend on the evolution time t_1. These terms gives rise to so called axial peaks in the 2D spectrum. The remaining terms give rise to cross (auto) peaks

$$M_{zA}^{cross} = -a_{AA} M_A^\circ \cos\omega_A t_1 \cos\omega_A t_2 \, e^{-t_1/T_{2A}} e^{-t_2/T_{2A}}$$
$$- a_{AB} M_B^\circ \cos\omega_B t_1 \cos\omega_A t_2 \, e^{-t_1/T_{2B}} e^{-t_2/T_{2A}}$$

(104)

After Fourier transformation the first peak on the r.h.s gives rise to a diagonal peak the second to a cross peak in the 2D spectrum.

94

ASSIGNMENT STRATEGY FOR NON EXCHANGEABLE PROTONS USING 2D-NOESY

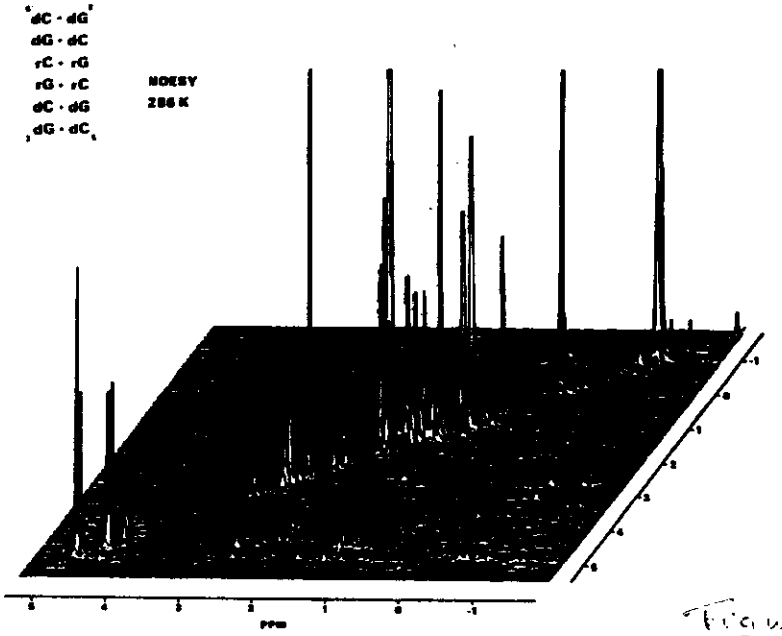

Figure 41

The method is applied to the double helical form of d(CG)r(CG)d(CG) A 2D-NOE spectrum obtained for this molecule is presented above. Diagonal peaks correspond (but are not equivalent) with

95

the convential 1D-spectrum; cross peaks represent Overhauser effects. A contour plot is shown below.

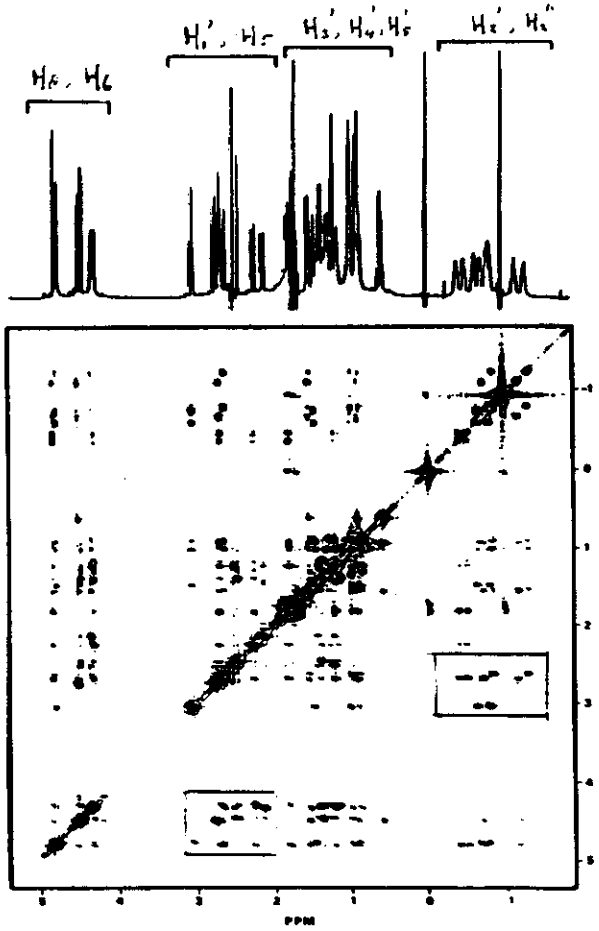

Figure 42.

96

The double helical molecule has a two fold axis of symmetry so that an identical set of resonances is obtained for each strand. In the contour plot blocs of cross peaks can be distinguished, which represent connectivities between certain groups of protons, e.g. the cross peaks between the C H8 and the C H6 protons on the one hand and the sugar H1''s on the other hand are enclosed in a box (see Fig 43). These crosspeaks can be used to perform a sequential assignment of the H1' sugar protons and the C H5 and C H8 non exchangeable ring protons. Consider Fig. 43

97

Figure 45

B-DNA

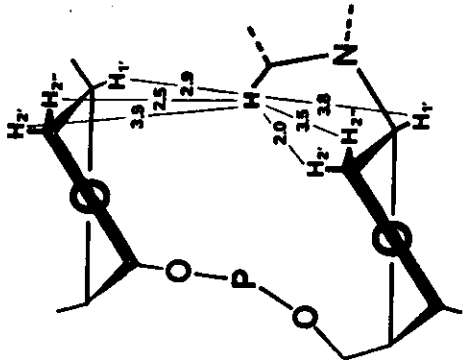

A-DNA

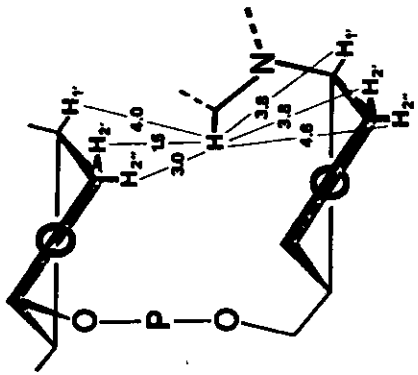

In Fig. 45 average distances between the purine H8 or pyrimidine H6 and the H_1', H_2', H_2'' (deoxy)ribose protons in A-DNA and B-DNA helices are presented.

In A-type as well as in B-type helical conformations the purine H8 and the pyrimidine H6 proton is close (within 4.0 Å) to its intranucleotide 1', 2' and 2" protons and also to the 1', 2', and 2" protons of the 5'-neighboring nucleotide but much less close to the sugar protons from the 3'-neighboring nucleotide.

Hence, intra- as well as inter-nucleotide (to the 5' neighboring sugar) Overhauser effects are expected in a 2D-NOE spectrum form the basis for sequential assignment. As can be gleaned from Fig. 44 each C8H8 or C6H6 proton must give rise to two

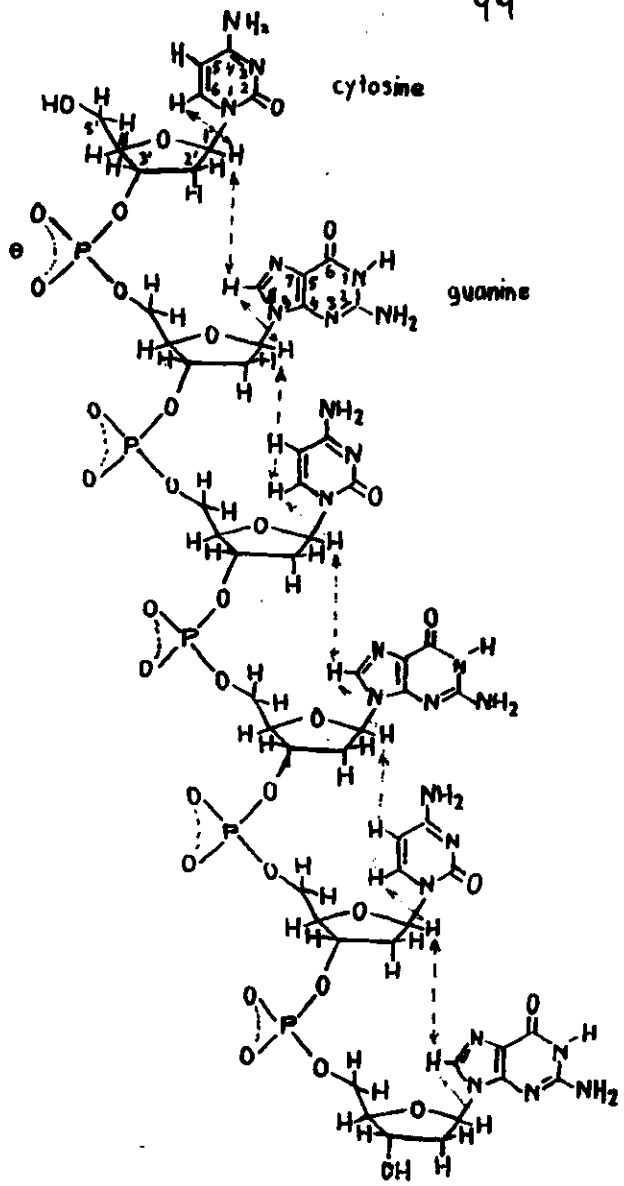

Figure 44

cross peaks except for CH6 proton of the 5' cytosine. This knowledge is used to start the sequential assignment, Fig 44

An expansion of the contour plot (Fig 45) is given, showing the cross peaks between the base protons and the H_1'-(deoxy)ribose protons (cross peaks in box). The drawn lines indicate how the sequential assigment is performed (Fig 45) (In the bottom panel a schematic representation of the same part of the 2D-NOE spectrum is presented; intranucleotide NOE's are marked O, internucleotide NOE's are marked X).

101

The assignment starts with the ringproton resonance (ring proton resonances are displayed along the vertical axis) which gives only one cross peak (coloured red) to sugar protons. As explained this must be the C H6 of the 5' terminal cytosine. Note that the cross peaks (coloured green) are from intra base NOE connectivities, i.e. CH6 ··· CH5 connectivities. (This can be checked independly in a spin decoupling or in a COSY experiment) We have now assigned the $C_1 H_6$ as well as the $C_1 H_1'$ proton resonances. Starting from the latter resonance we see it is

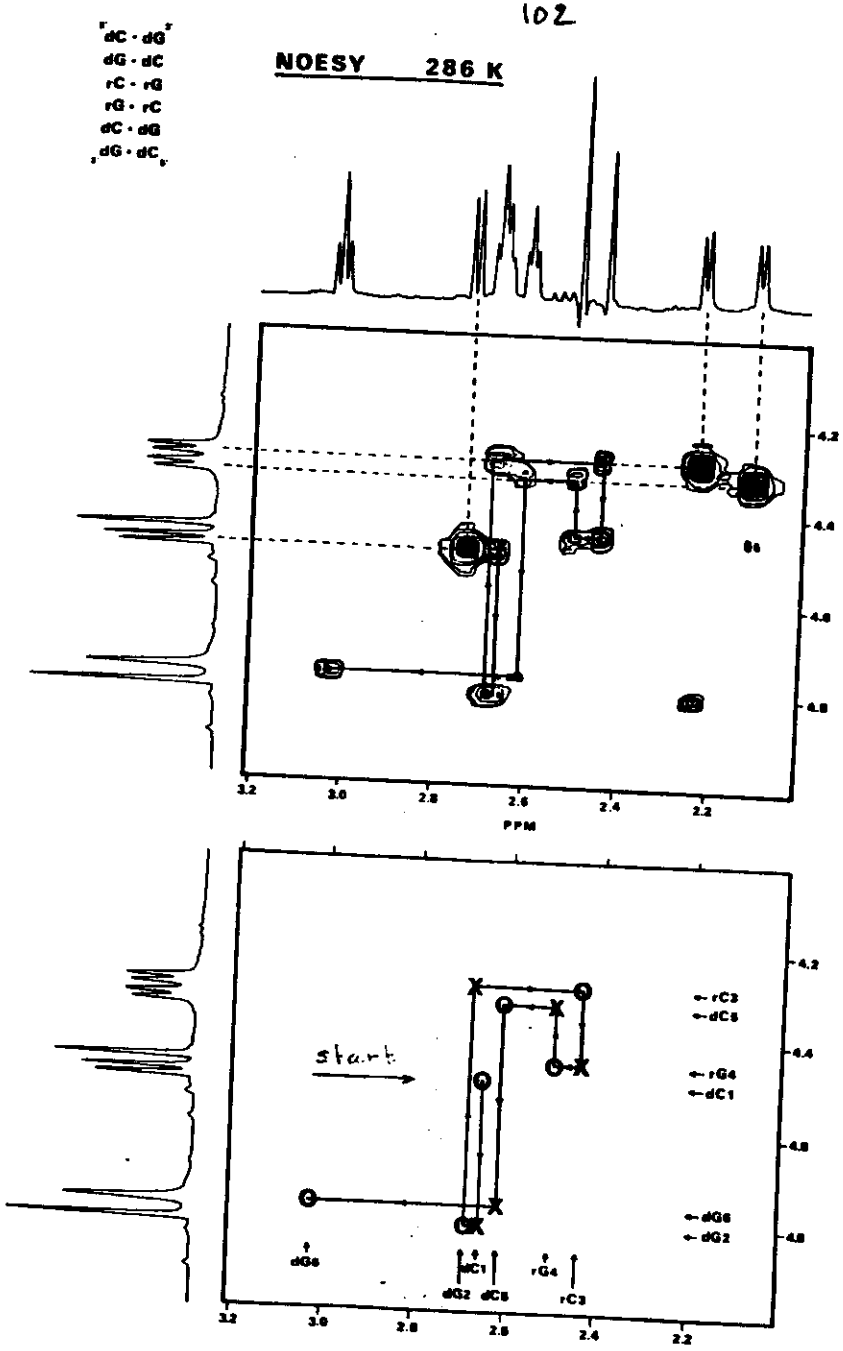

Fig. 4 5

connected via a cross peak (X below the red cross peak in the bottom panel) to the dG H8 resonance of guanine 2. We then proceed along the horizontal axis to the cross peak connecting the d G(2) H8 and d G(2) H1' resonances. From now on the procedure becomes repetitive: d G(2) H1' is interconnected to r C(3) H6 which is in turn connected to r C(3) H1' (at 2.44 ppm) and hence forward. In this way all 1' protons and base protons are assigned. In a similar way the 2' (and 2") protons can be assigned. Interpretation of the corresponding

spectrum is also possible by making use of the connectivities between the 1'- and the 2' (and 2") protons (cross peaks in green box, Fig 42.) Using the remaining connectivities the other sugar proton resonances can be assigned as well.

References:

Haasnoot et. al. Journal of Biomolecular Structure and Dynamics, 1, 131 (1983).

STRUCTURE OF DOUBLE STRANDED d(CG) r(CG) d(CG) IN SOLUTION

How can the assignments be used to obtain structural information about the double helical molecule? The molecule is a DNA - RNA hybrid and it is interesting to know whether an A - type helix or a B - type helix prevails. Recall that it is generally accepted that A - type helices are characterized by N - type (C3' - endo) and B - type helices by S - type (C2' - endo) sugar conformations. Having assigned all sugar resonances the J - coupling of the individual sugar protons can be determined.

	$J_{1'2'}$	$J_{1'2''}$	$J_{2'3'}$	$J_{2''3'}$	$(J_{1'2'} + J_{1'2''})$	$(J_{1'2''} + J_{2''3'})$
d C(1)	7.6	6.2	6.9	3.4	13.8	9.6
d G(2)	9.4	5.1	5.1	1.3	14.5	6.4
r C(3)	≤1	–	–	–	–	–
r G(4)	≤1	–	–	–	–	–
d C(5)	5.3	6.5	6.2	7.0	11.8	13.5
d G(6)	7.1	6.6	6.1	4.1	13.7	10.7

Coupling constants observed for the protons in the sugar rings of d(CG) r(CG) d(CG).

The 1' proton resonances of the central ribose moieties are sharp singlets. Hence $J_{1'2'} \leq 1$ Hz for both these ribose rings. This value corresponds with a conformationally

pure N-type ribose ring. Therefore the central part of the molecule adopts an A-type double helical conformation.

Analysis of the coupling constants of the other sugar ring in terms of an N/S equilibrium using (see eq. 46)

$$\%S = (17.8 - J_{1'2''} + J_{2''3'})/10.9$$

yields the N/S distributions indicated in Fig. 46

Population distribution of N/S sugar conformations. Hatched (red) regions indicate the N(C3' endo) population percentage for the corresponding nucleotide.

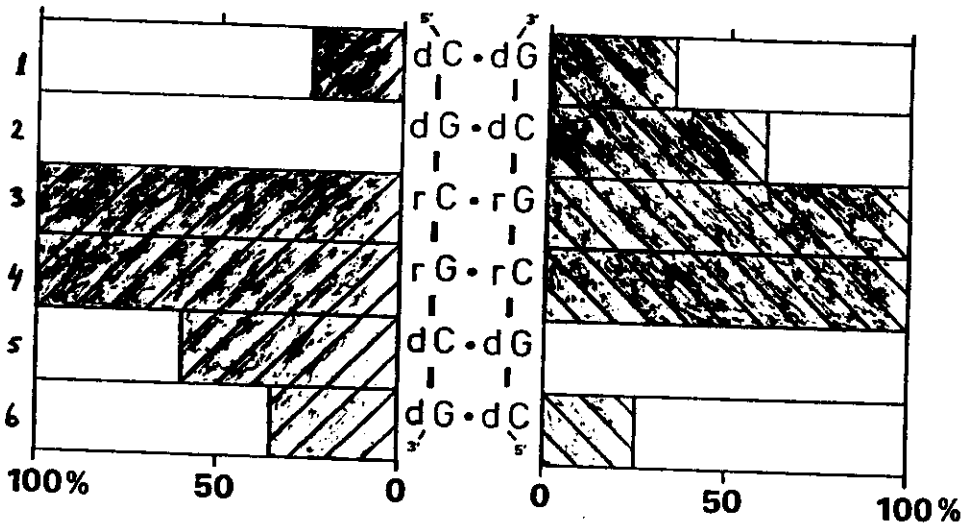

d C(5') has a suprizing large (60%) N type population; d C(1) and d G(6) have a preference for an S type conformation (fraying may

may influence the population. dG(2) adopts a pure S-conformation.

Hence, deoxyribose rings exhibit conformational freedom in contrast to ribose rings. Conformational freedom for deoxyribose rings has been observed in many model systems.

So far the Overhauser effects have been used for sequential assignment. They can also be used in a semiquantitative manner to distinguish different types of helices in solution.

IV IMINO PROTON EXCHANGE AND THE STABILITY AND DYNAMICS OF DOUBLE HELICES

If the temperature of a double helical DNA (or RNA) molecule is raised sufficiently, the double helix is disrupted or melted out (the process resembles a phase transition). Concommitant with the melting the imino proton resonances disappear from the spectrum very often preceded by line broadening.

Example: the helix coil transition of the hexadecamer d(ATCCTATTTTAGGAT)

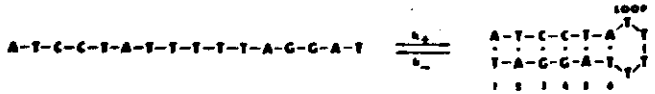

Helix to coil transition of hexadecanucleotides of which the imino spectra are shown as a function of temperature.

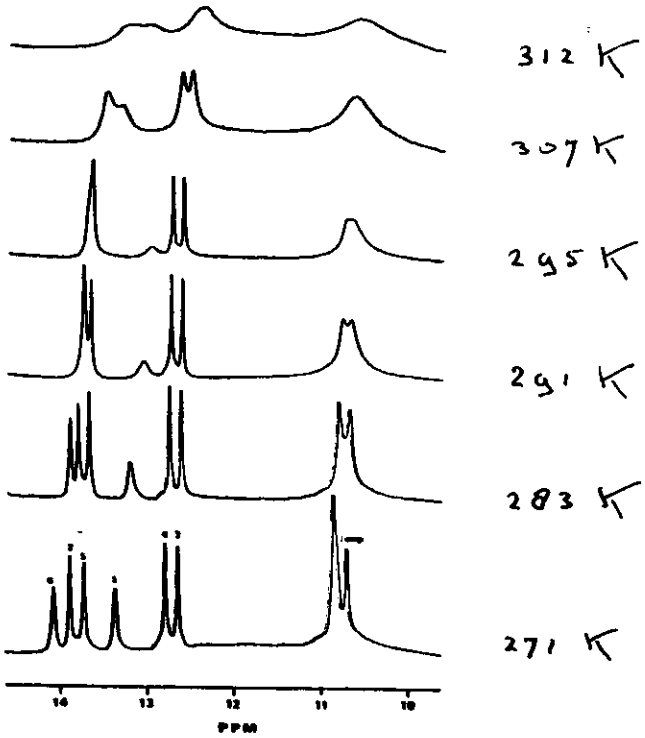

The broadening and shifting of iminoproton resonances will be described with the following model for iminoproton exchange

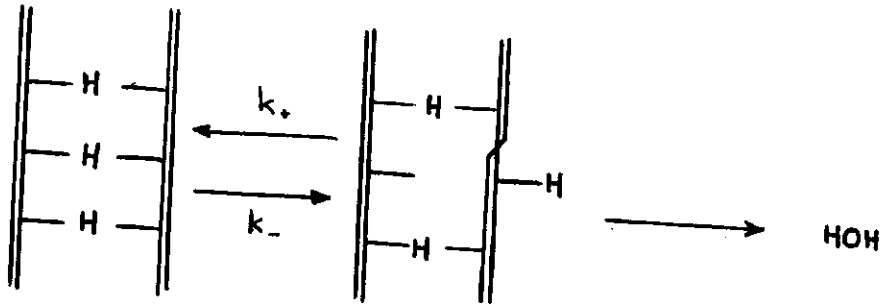

The first step is basepair opening:

The second step is proton exchange:

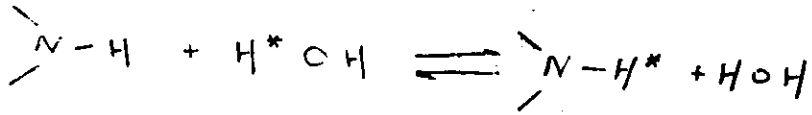

This step may be catalyzed by base or buffer.

$$\geq N\text{-}H + B \underset{}{\overset{k_c}{\rightleftharpoons}} \geq N^- + BH^+$$

The overall rate constant for proton transfer from the base paired state to buffer (or base) is:

$$k_{ex} = \frac{k_- k_c [B]}{k_+ + k_c [B]}$$

If $k_c [B] \gg k_+$:

$$k_{ex} = k_-$$

exchange is <u>opening limited</u>

If $k_c [B] \ll k_+$

$$k_{ex} = \frac{k_-}{k_+} k_c [B] = K_{diss}\, k_c [B]$$

exchange depends on the equilibrium

dissociation constant and on the buffer (or base) concentration; this is <u>the pre equilibrium limit.</u>

The rate constant k_c is related to the difference in pK values between the $\geq N\text{-}H$ moiety and the base or buffer molecules (ions) by

$$k_c = k_f \frac{10^{\Delta pK}}{1 + 10^{\Delta pK}}$$

with $\Delta pK = pK(BH^+) - pK(\geq N\text{-}H)$

(Englander et al. Ann. Rev. Biochemistry 41, 903, 1972)

In NMR the imino proton exchange model represents a three site exchange problem.

The iminoproton resonance "jumps" from the closed state resonance position to that of the open state and subsequently to the water position. Consider the limiting situations:

a) slow exchange between the helix and coil state

$$\tau_{hc}^{-1} = \pi \Delta\nu_{\frac{1}{2}} = k_-$$

τ_{hc} is lifetime of the imino proton in the basepair.

$\Delta\nu_{\frac{1}{2}}$ is line broading

measured at half height of the iminoproton resonance. In this exchange limit, the resonance position coincides with that of the iminoproton in the double helical state.

b) fast exchange between helix and coil; for this situation there are two possibilities

i) exchange with water (or buffer) occurs virtually every time the imino proton is not hydrogen bonded (i.e. base pair disrupted).

$$\tau_{hc}^{-1} = \pi \Delta\nu_{\frac{1}{2}} = k_-$$

as for the slow exchange

ii) the imino proton interchanges many times before exchange to water takes place

$$\pi \Delta\nu_{\frac{1}{2}} = f_c \tau_{cw}^{-1} = K_{diss} k_c [B]$$

f_c is the fraction of imino proton in the coil form; τ_{cw}^{-1} is the transition probability per unit time that the iminoproton is transferred from the open state to the buffer ions.

The resonance position of the imino proton is given by

$$\bar{\omega} = f_h \omega_h + f_c \omega_c$$

$\bar{\omega}$ is the observed resonance

position, ω_h is the imino proton resonance position in the base paired state and ω_c is the position in the open state; f_h and f_c are the fractions in the basepaired and coiled state respectively. Hence, line broadening is not determined by the lifetime of the basepair but by the "leakage" of the imino protons to buffer (or base, e.g. hydroxyl ions); this is the pre equilibrium situation.

Example : the self complementary hexa nucleotide d(ATGCAT)

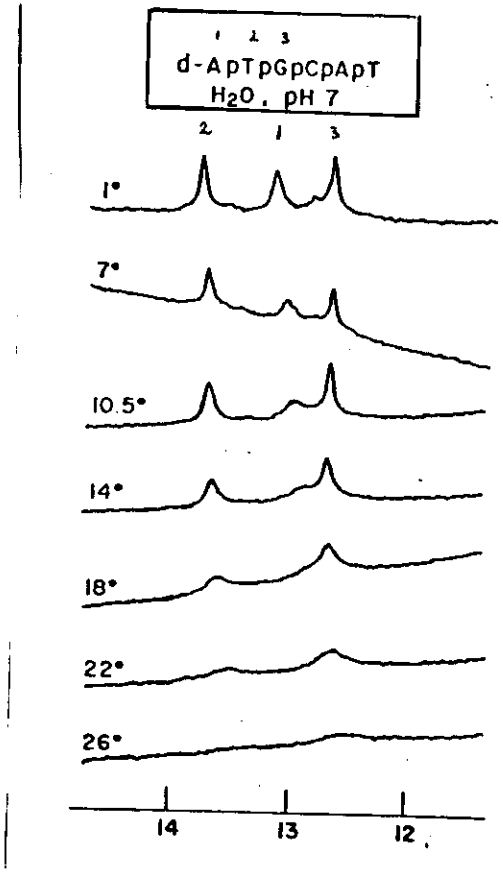

Resonance 1 shifts and broaclens suggesting $\pi \Delta\nu_{\frac{1}{2}} = K_{diss}\, k_c\, [B]$: this is confirmed in the following experiment:

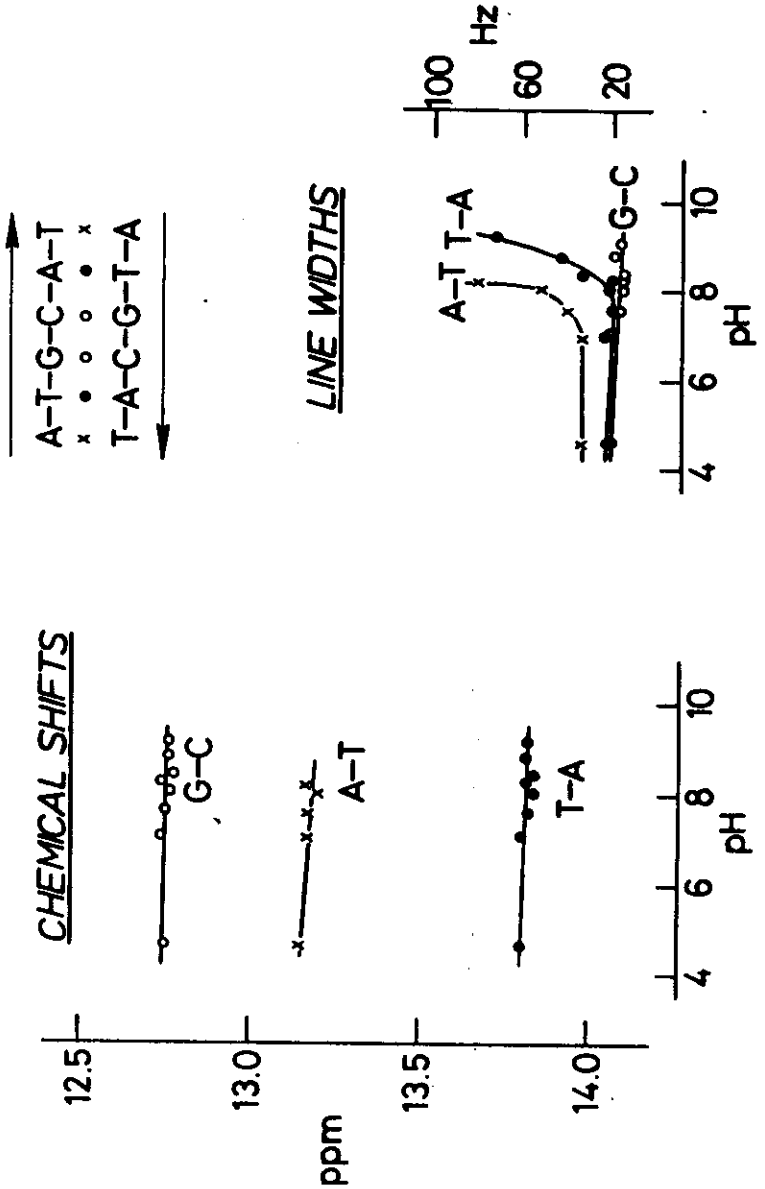

Measurement of linewidth and shift as a function of pH.

The line width of the iminoproton resonances of the terminal and internal AT pairs depend on pH ; the exchange can be described by a pre equilibrium situation. The base pairs are opening and closing very rapidly a process called fraying

The broading and shifts observed in Fig ... are plotted in Fig ... as a function of temperature.

The equilibrium dissociation constant for the opening of the terminal base pair can be calculated from

$$K_{diss,r} = (\omega_{Th} - \bar{\omega}_r)/(\bar{\omega}_T - \omega_{Tc})$$

Figure :

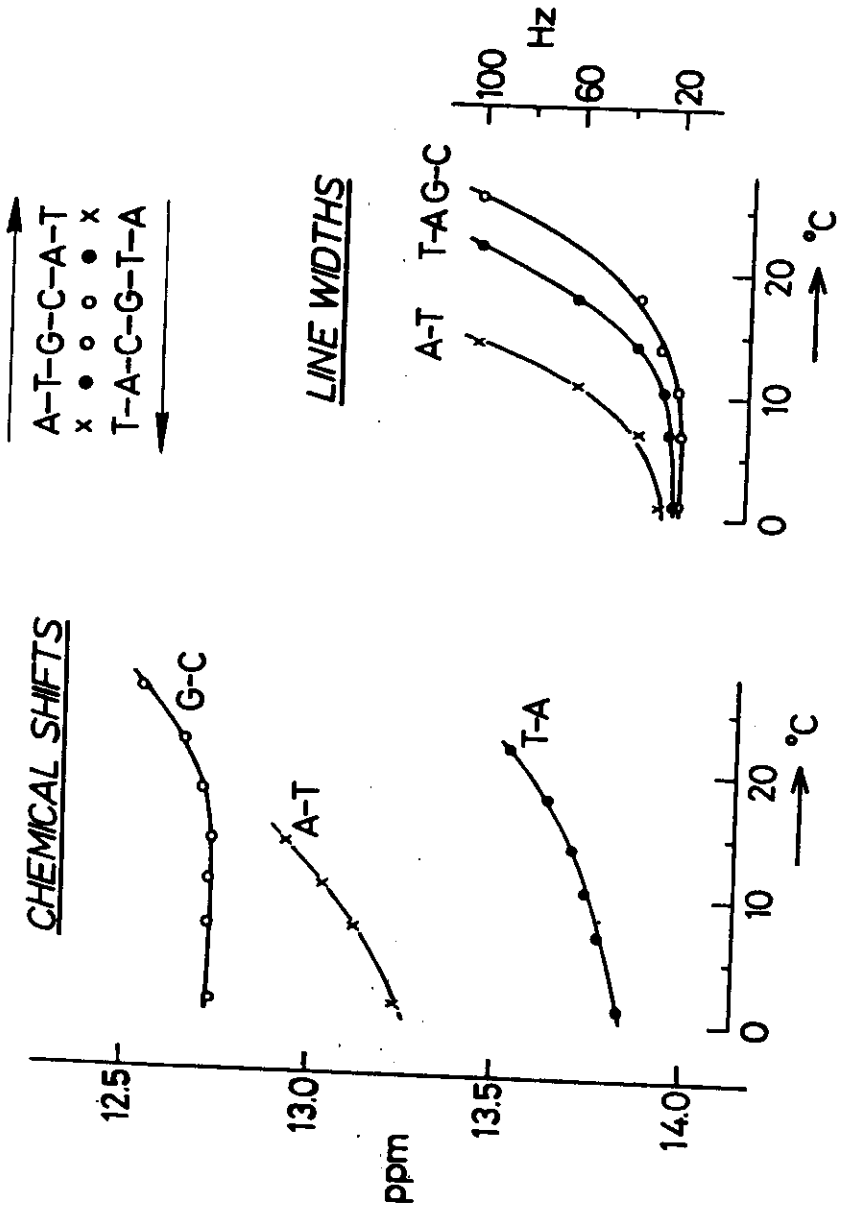

where $\bar{\omega}_T$ is the position observed for the terminal iminoproton resonance; ω_{T_h} is the resonance position for the intact base pair ω_{T_c} is the position for the open state.

From the line width and the hydroxyl ion concentration the reaction rate constant k_c can be calculated. This yields $k_c \geq 0.5 \times 10^{10}\ M^{-1}s^{-1}$

Hence, exchange from the open state to hydroxyl ions is diffusion limited in accordance with predictions from Eq. ..

The opening of the internal AT basepair is not independent from the opening of the terminal basepair. The helix disruptaire proceeds from the ends to the center; only those internal basepairs open for which the terminal base pairs have already been disrupted.

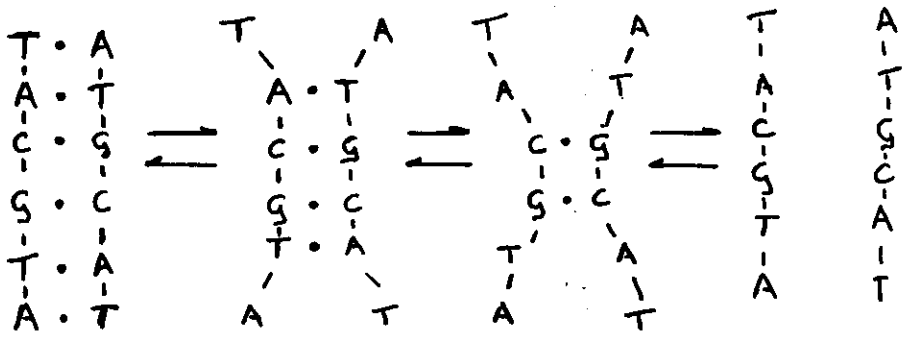

The equilibrium constant for the internal AT pair is (accounting for this effect):

$$K_{diss,int} = \frac{(\omega_{Tc} - \omega_{Th})(\bar{\omega}_i - \omega_{ih})}{(\omega_{ic} - \omega_{ih})(\bar{\omega}_T - \omega_{Th})}$$

$\bar{\omega}_i$ is the observed resonance position of the internal AT pair iminoproton ω_{ih} and ω_{ic} is its resonance position in the intact base pair and in the open state respectively.

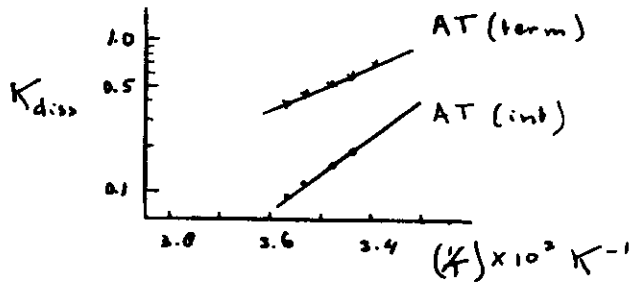

Plots of the log of K_D versus $1/T$ yield the reaction enthalpy for base pair opening according to

$$\frac{\partial \ln K_{diss}}{\partial\ 1/T} = -\frac{\Delta H_{diss}}{R}$$

126

In this way we obtain

ΔH (AT term) = 6.1 kcal/mol

ΔH (AT int) = 11.8 .

Above 20°C, where the GC resonances start to broaden, also shifts are observed for these resonances, meaning that the exchange limit is not strictly opening limited. This limit can be obtained again by increasing the buffer concentration. In the latter situation

$$\pi \Delta \nu_{\frac{1}{2}} = k_d - k_{6,2}\ c_{2,c}^{-1}$$

where k_d is the dissociation rate of the total double helix $k_{6,2}$ is the equilibrium dissociation

constant from the intact helix to a particle containing only two GC pairs and $\tau_{2,0}^{-1}$ the dissociation rate of these two remaining GC pairs. Since the activation energy of double helix formation is close to zero it is to be expected that (according to Eq.) the activation energy of dissociation is close to the dissociation reaction enthalpy. This is indeed following from the experiment (see Fig).

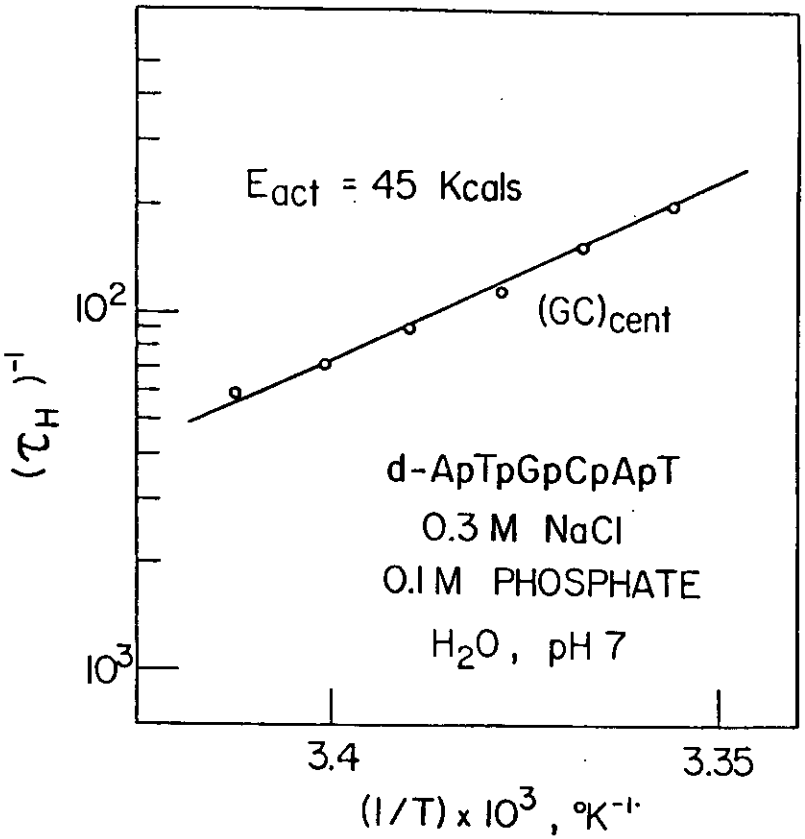

Figure Activation energy determined from the line broadening of the GC pairs.

Combination of iminoproton exchange and T-jump kinetics

In the preceding section it was concluded that the broading of the resonances of the central GC base pair was proportional to the dissociation rate of the total helix. This can be verified experimentally by a combination of NMR imino exchange studies and T-jump kinetics. As an example we will discuss the experiments performed for a 49 nucleotide fragment from the 3' end of 16 S ribosomal RNA from E. coli.

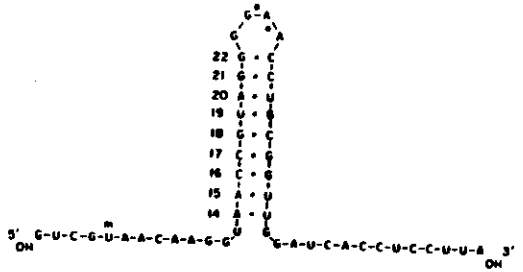

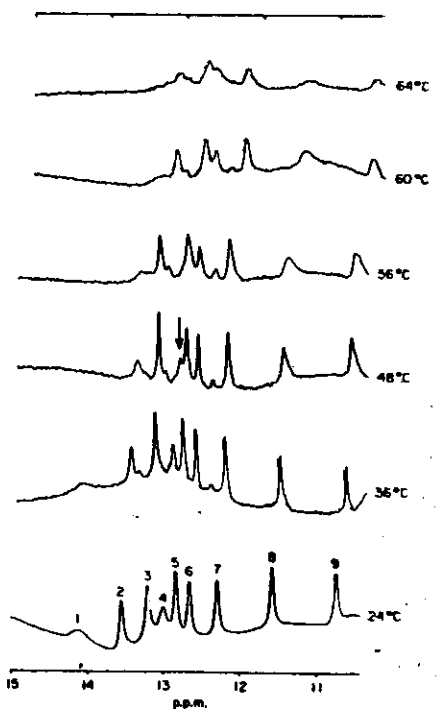

The assignment of these resonances has been carried out by means of 1D NOE experiments as discussed for yeast $tRNA^{Phe}$ (Hens et al. J. Mol. Biol 170, 939, 1983). In NMR melting experiments the resonances of the GC base pairs 3, 5, 6 and 7 are seen even at 64°C indicating that these are the most stable base pair. The resonance of AU 2 broadens at much lower temperature. The line broadening of the resonances of AU 2 and GC 3 is plotted as a function of temperature in Fig. ...

The apparent base pair

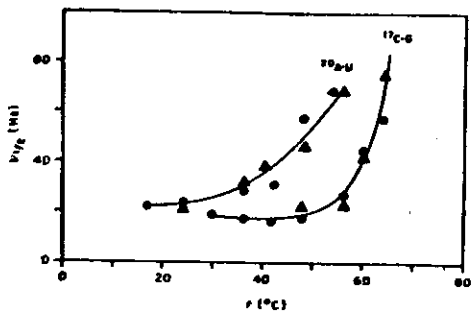

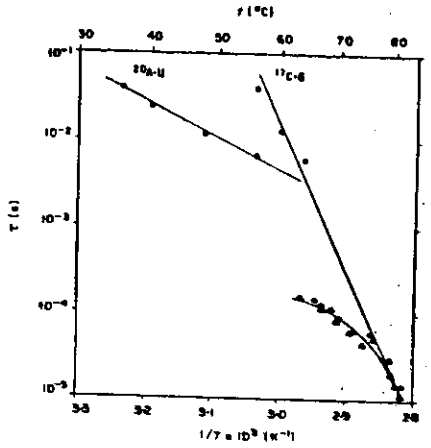

131

dissociation rates calculated from the line broadening are plotted in Fig.. together with the relaxation rates obtained by means of T-jump experiments (temperature jump experiments).

In a temperature jump experiment the temperature of a sample is very rapidly (in μs) increased by a few degrees.

If we are studying a helix to coil transition in this way, the system will adjust to the new temperature, but not as fast as the temperature jump. This process can be followed by monitoring the

absorption of the sample at 260 nm (melting is accompanied by a hyperchromicity effect).

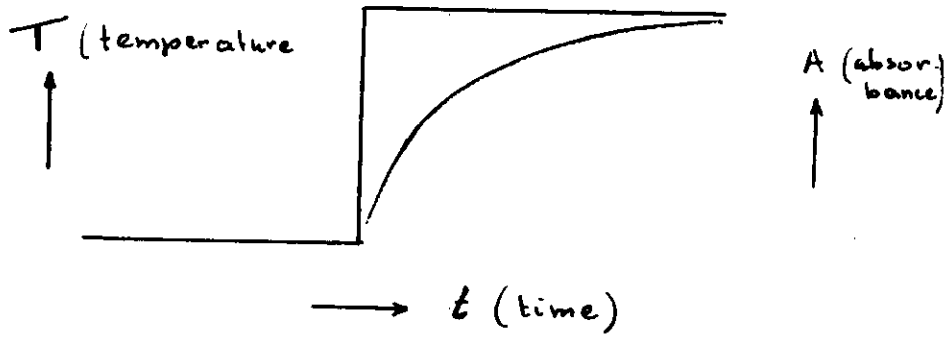

The adjustment to the new temperature can be characterized by a relaxation time τ,

For intramolecular reactions, e.g. hairpin formation

$$\tau^{-1} = k_+ + k_-$$

For low temperatures (below the melting temperature) τ^{-1} is

determined by the helix formation rate k_+. At high temperature (above the melting temperature) τ^{-1} is determined by the helix dissociation rate. For the ribosomal fragment the melting temperature is ~ 70°C. Extrapolating the dissociation rates obtained from T-jump to temperatures were a linebroadening is observed for the iminoproton resonances we see that the dissociation rate determined for the GC resonance is obtained within experimental accuracy. This demonstrates that the linebroadening observed for the GC pairs is proportional to the dissociation

rate of the <u>total</u> helix as expected (see previous section).

Interestingly, the exchange of the AU basepair iminoproton is not opening limited. It is however flanked by a GC pair which is more to the end of the double helix. The exchange of the iminoproton of this basepair is determined by the lifetime of the double helix (i.e. is proportional to the helix dissociation rate). Apparently, the

A · U

U · G

forms a spot within the double helix with special exchange properties.

T_1 RELAXATION AND IMINO PROTON EXCHANGE.

Determination of exchange rates by means of the line broadening of imino proton resonances is limited to a restricted temperature range. By means of T_1 relaxation measurements this range can be extended significantly to lower temperatures (below the melting temperature). The measurements are performed with the following pulse sequence

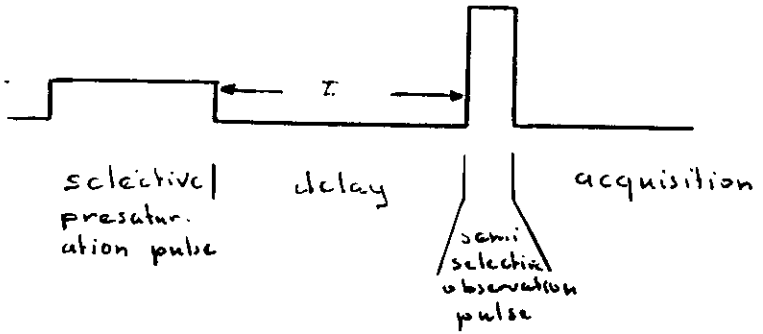

As an example consider resonances from the acceptor stem of yeast $tRNA^{Phe}$

Reason: increasing concentrations of spermidine broadens the imino proton resonances of the GU basepair in the acceptor stem (see Fig) These cations are known to stabilize double helical regions in DNA and RNA molecules and are not supposed to disrupt basepairs.

In fig . T_1 measurements carried out for the imino proton resonance of GC's are presented. According to equation (18) a plot of the

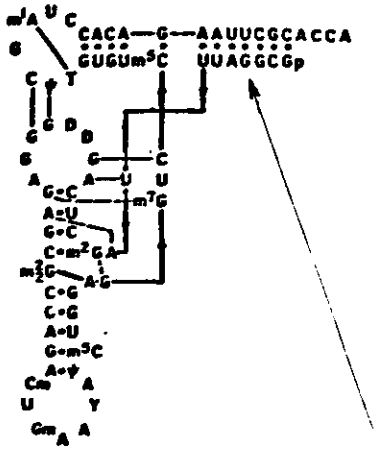

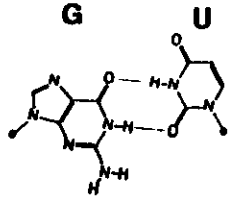

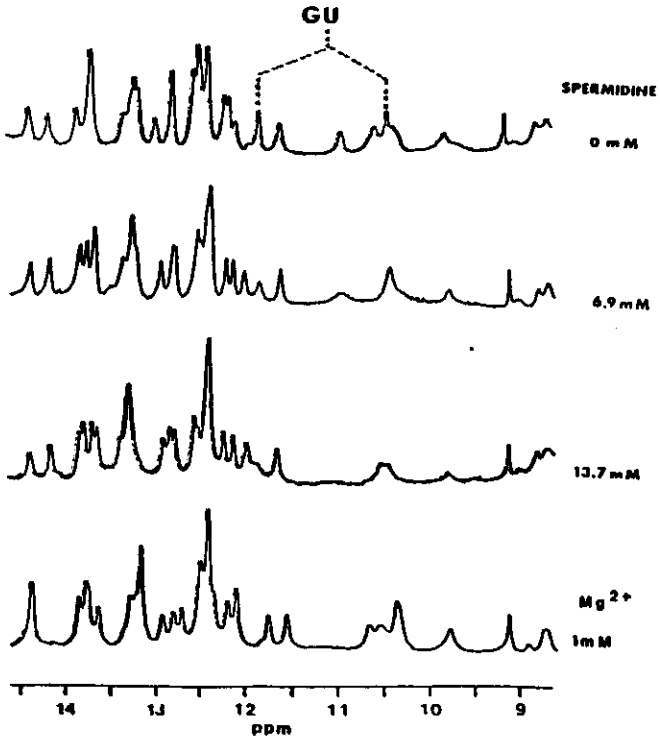

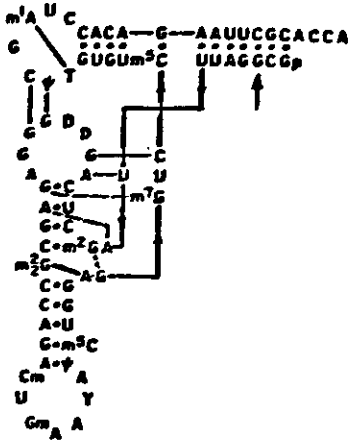

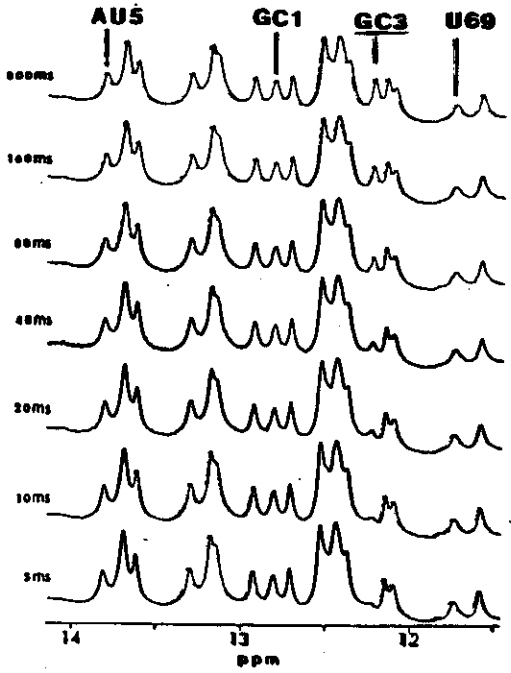

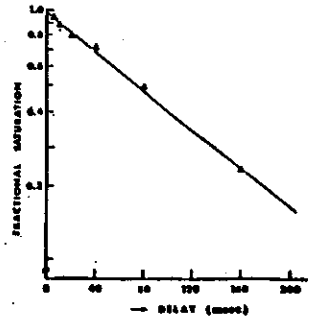

$$\ln\left[\frac{M_z - M_s}{M_0}\right] = -\frac{1}{T_1}$$

log - intensity versus delay time (after saturation) yields a straight line from which T_1 can be calculated

T_1 has been measured for the imino protonresonances of GC1, GC3 GU4 and AU5 (well resolved resonances) as a function of temperature (Fig)

$$T_{1\,obs}^{-1} = T_{1\,magn}^{-1} + k_{ex}$$

The reciprocal of the observed T_1 is equal to the magnetic relaxation ($T_{1\,magn}^{-1}$) plus a term characterizing the exchange of the imino protons to water.

The magnetic relaxation is within the temperature range

$$T_1^{-1} = T_{1\,mag}^{-1} + k_{ex}$$

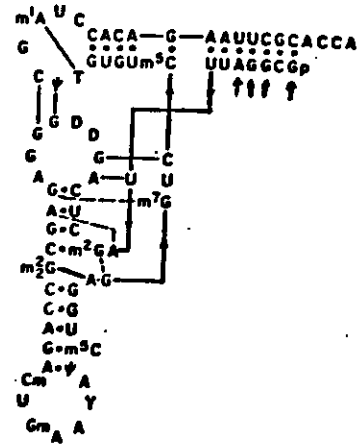

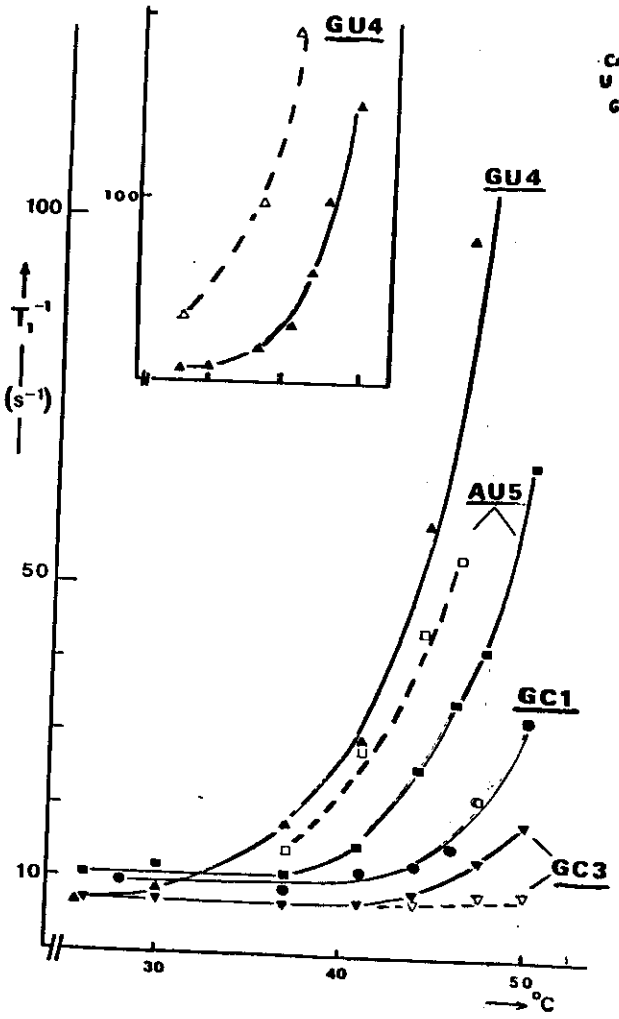

considered, independent of temperature. Below 35°C this term is responsible for the observed T_1 (except for the GU basepair). The relaxation rate amounts to $10\ s^{-1}$ a value found by different investigators for iminoproton relaxation. At higher temperatures exchange processes start to contribute to the observed relaxation. This is most pronounced for the GU 4 basepair, least for the GC 3 basepair. When sufficient spermidine is added and the experiment are repeated it is seen that

for GU 4 and AU 5 exchange is increased, the exchange of GC 1 is not influenced, while the exchange of GC 3 is slowed down.

Explanation: spermidine binds to the acceptor stem; exchange of the iminoprotons can be catalyzed by spermidine. The overall exchange is in this case described by

$$k_{ex} = K_{diss}\, k_c\, [B]$$

Upon binding of spermidine K_{diss} does not change or decreases; the term $k_c\,[B]$ increases. If the latter changes outweigh the changes in K_{diss}

the relaxation rate will increase upon addition of spermidine. Analogously to the ribosomal RNA fragment also in tRNA the sequence

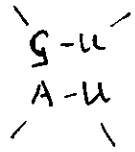

forms a spot in the double helix with special exchange properties